Monitoring of Bridge Deformations - Proof of Concept

Technical Report, December 2021

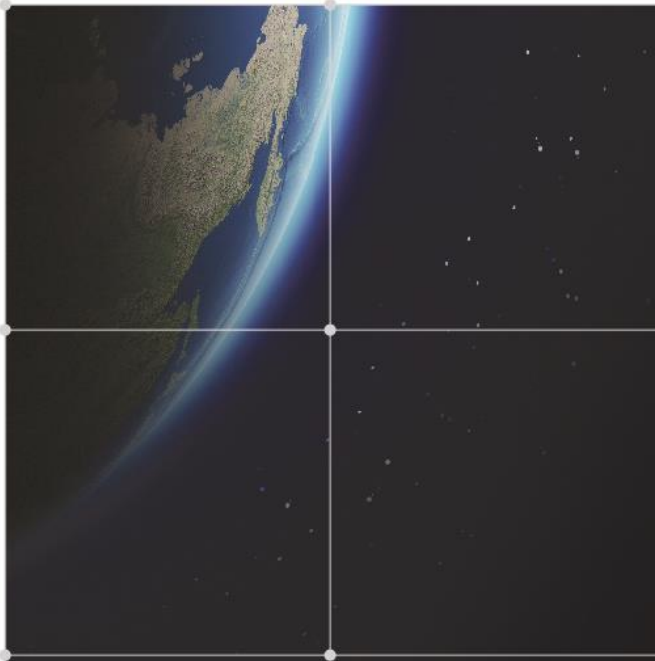

TRE ALTAMIRA
A CLS Group Company

Bijlage 7/1

Client:

Leen Devos

Ministeries van de Vlaamse Gemeenschap

Departement Mobiliteit en Openbare Werken - Afdeling Geotechniek

Reference:

Title:	Monitoring of Bridge Deformations – Proof of Concept
TRE ALTAMIRA Project Reference:	JO21-1613-ES
TRE ALTAMIRA Delivery Reference:	ES4710A2S / ES4711A2S

Prepared by:

TRE ALTAMIRA

Author:	Eric Henrion, Javier Garcia, Pablo Blanco
Verified by:	Jordi Sanchez, Ségolène Duprat
Approved by:	Stefano Cespa
Date:	17 December 2021
Version:	1.0

Table of Contents

Table of Illustrations

Acronyms and Abbreviations

AOI	Area of Interest
ATS	Average Time Series
DEM	Digital Elevation Model
DS	Distributed Scatterer
GIS	Geographic Information System
InSAR	Interferometric Synthetic Aperture Radar
LOS	Line of Sight
PS	Permanent Scatterer
SAR	Synthetic Aperture Radar
SNT	Sentinel-1 satellite
SqueeSAR®	The most recent InSAR algorithm patented by TRE
TS	Time Series
TSX	TerraSAR-X satellite

1. Introduction

The Flemish public administration (Department of Mobility and Public Works / Geotechnics Division) manages more than 2 500 bridges and wants, by means of this innovative contract, to find out whether an InSAR (Interferometric Synthetic Aperture Radar) analysis could prove an alternative or offer added value compared to the current method used for monitoring bridge deformations (via levelling). The other aspect of this project is to provide a clear insight of the added value brought by high-resolution radar images for the analysis and into the percentage of bridges that can be monitored using InSAR analysis.

An initial Proof Of Concept (POC) is implemented and focused on a limited area, north of Brussels. It consists of the analysis of 21 bridges of different orientations, lengths, materials, and year of construction (Figure 1). The analysis of these bridges and their surroundings will be conducted using Sentinel-1 (SNT) and TerraSAR-X (TSX) SAR satellites and the patented SqueeSAR® algorithm to provide the state of the art of surface ground movements. The SNT images cover the period from November 2014 to October 2021, and the TSX images cover the period from June 20214 to March 2016.

In addition of deformation and deformation rates from each study, further analysis will be carried out over the bridges in order to extract all available information about their behaviour. Seasonal amplitude will be extracted from the SqueeSAR® to allow the client to analyse any correlation between surface deformation and temperature. Trend Variation analysis on the measurement point time series will be conducted in order to detect abnormal behaviour within the studied area. Trend Change Detection analysis will also be conducted on amplitude images to allow the client to analyse any correlation between construction work and measurement point availability. Finally, an Alerting System will be proposed based on the surface deformation analysis.

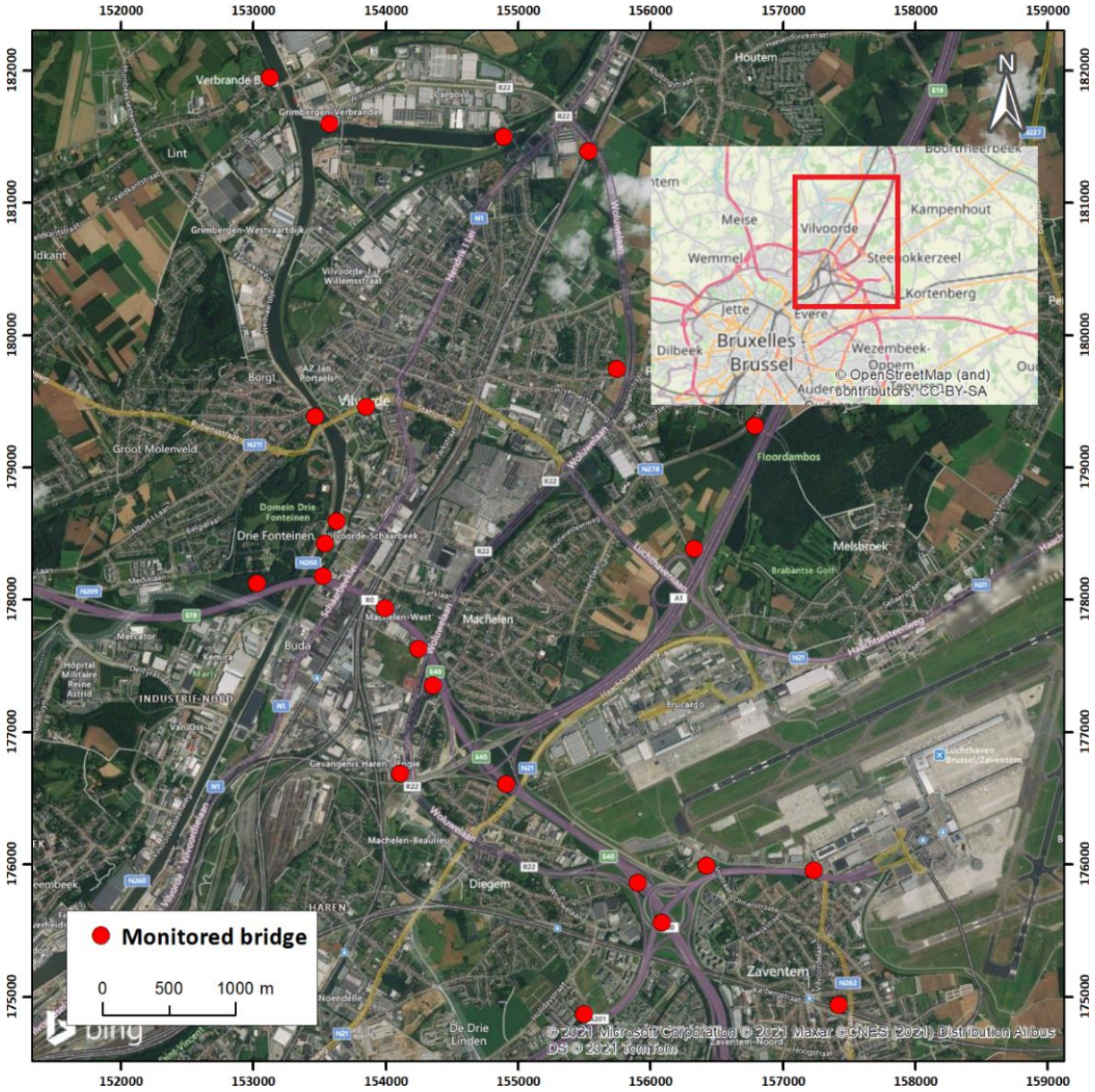

Figure 1. Area Of Interest (in red) of the POC, north of Brussels. The bridge locations are represented by red circles.

2. InSAR principles

2.1. Permanent Scatterers and Distributed Scatterers

SqueeSAR® is the proprietary multi-interferogram technique patented by TRE ALTAMIRA, providing high precision measurements of ground displacement by processing multi-temporal SAR images (at least 15-20) acquired over the same area, with the same mode and geometry.

By statistically exploiting the imagery, SqueeSAR® singles out measurement points (MP) on the ground that display stable amplitude and coherent phase throughout every image of the dataset. The MPs belong to two different families (Figure 2):

- Permanent Scatterers (PS): point-wise radar targets characterized by high stable radar signal return (e.g. buildings, rocky outcrops, linear structures, etc.).
- Distributed Scatterers (DS): patches of ground exhibiting a lower but homogenous radar signal return (e.g. uncultivated land, debris, deserted areas, etc.).

The density and distribution of the MP is related to the resolution of the SAR images used, the surface characteristics, and the topography of the area. In general, the MP density increases with the satellite spatial resolution and the presence of man-made structures and decreases with the presence of vegetation. The highest density is reached over urban and bare areas, while it is lower over areas deeply vegetated, affected by strong reflectivity changes with time or where the satellite visibility is limited (shadowing). Of course, no measurement points are identifiable over water.

As seen in Figure 2, a DS corresponds to an extensive area where back scattered energy is weaker than a PS but is statistically homogeneous within the area. Unlike a PS, where the backscattered energy is high and concentrated in a small area, the radar echo intensity for a pixel belonging to a DS is usually much lower. Estimating deformation based on individual pixels would not be possible for cells corresponding to a DS as their low signal-to-noise ratio (SNR) restricts obtaining reliable motion estimates. However, the SqueeSAR® algorithm performs a sophisticated space-time filtering on areas where pixels exhibit similar incident radar signals which results in reducing the noise associated with a DS. The results are deformation estimates obtained from PS and DS that are of comparable quality.

Atmospheric components are estimated on a set of good radar targets, now selected among both PS and DS. However, the information estimated for the DS is associated not to a single point target but to a homogeneous patch of ground. The main advantage offered by the SqueeSAR® approach is the increase in spatial density of MPs. A higher density of radar targets generally allows a better estimation of the atmospheric disturbances and therefore better estimation of displacement.

Information provided by SqueeSAR® is particularly effective in non-cultivated areas, rocky deserts, debris fields and non-urbanized areas. This information can be particularly useful in delimiting areas affected by ground deformation or displacement phenomena.

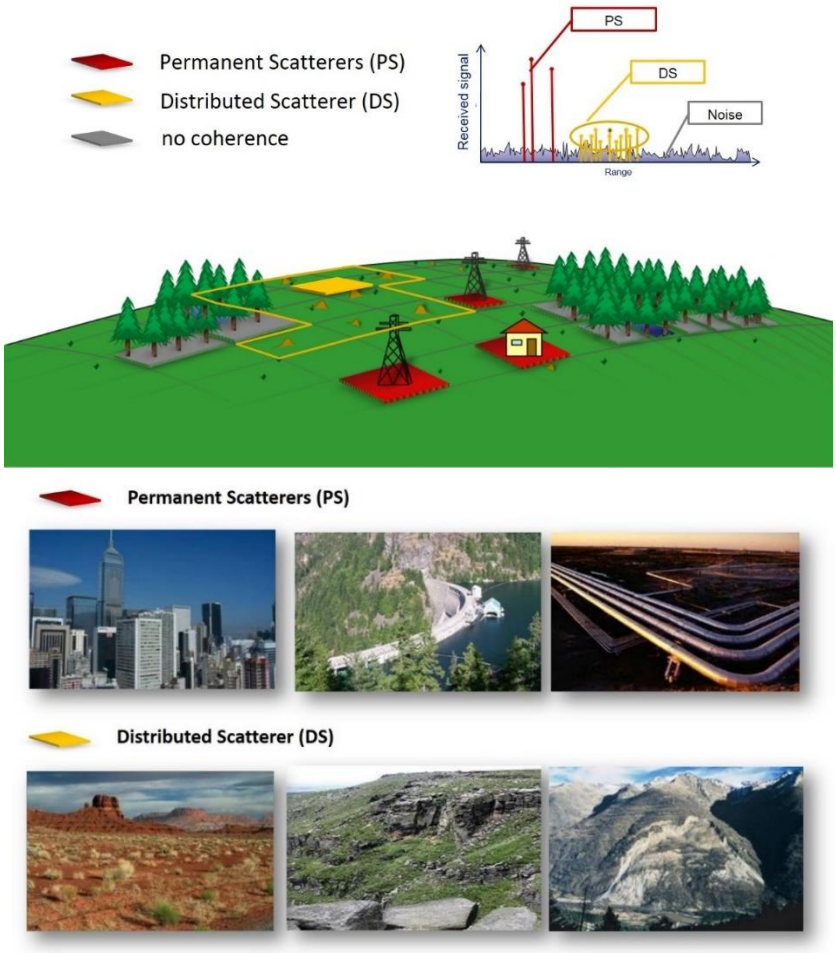

Figure 2: Schematic showing the distribution of PS and DS. PS are identified as single objects returning a strong signal to the satellite. DS are homogeneous areas or scattered outcrops. Areas heavily covered by vegetation do not return the satellite signal.

2.2. SqueeSAR® Analysis

In InSAR analyses, all measurements are in 1D along the sensor's Line Of Sight as the true vector of deformation is projected to the LOS. The same deformation will produce different interpretations when viewed from different point of view or angle (Figure 3). The LOS angle θ represents the inclination to the vertical.

The LOS deformation rates are calculated from a linear regression of the ground movement measured over the entire period covered by the satellite images. Each measurement point (MP) corresponds to a Permanent

Scatterer (PS) or a Distributed Scatterer (DS), colour-coded according to its annual rate of movement and direction. In a descending LOS analysis, negative values (red) indicate surface deformation away from the satellite (i.e., subsidence and/or westward movement), while positive values (blue) indicate surface deformation towards the satellite (i.e., uplift and/or eastward movement).

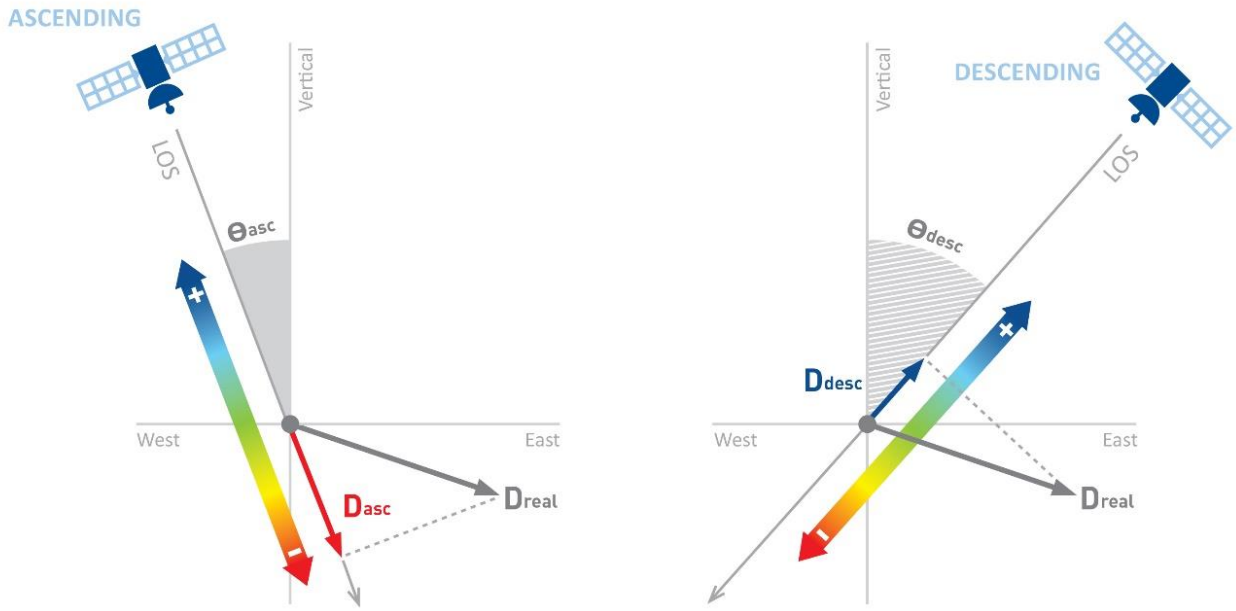

Figure 3: SqueeSAR® measures the projection of real movement (D_{real}) along the LOS. The same real movement (D_{real}) will produce a different value from a different LOS (different inclination or different acquisition geometry).

Deformation measurements obtained by the SqueeSAR® algorithm are differential in space and time. Measurements are spatially related to the reference point (REF) like any geodetic network, and temporally to the date of the first available satellite image.

The REF is assumed to be motionless and selected for its radar properties and motion behaviour. It corresponds to a radar target with low phase noise in all the scenes of the imagery, not affected by displacement rate variations (non-linear movement or cyclical deformations) in the covered period. This means that the REF can still be affected by a linear movement related to regional deformation phenomena. The selection of the REF is imagery dependent. If the imagery changes (by the number of scenes or time span), the MP selected as the REF can change. Furthermore, the geographic location of the chosen MP as REF is not considered.

2.3. Measurement Point displacement accuracy

The precision of SqueeSAR® displacement measurements depend on performing a correct phase unwrapping and estimating the atmospheric contributions. Since the elaboration is statistically based, the main factors influencing the accuracy are not only related to the quality of each single acquisitions but also to the quality of the entire processed dataset.
The atmospheric noise component for each acquisition depends on:

- The time of acquisition: there is a greater atmospheric noise during daytime.
- The acquisition geometry: higher LOS angle implies a longer distance to cover and therefore more atmospheric disturbance.
- The distance from the reference point.

The quality of the processed dataset depends on:

- The number of processed images: higher the number of images, higher the quality of estimations.
- The length of the interval analysed: the longer the time span, the higher the quality of the estimations.
- The temporal continuity of acquisitions: the higher the regularity of acquisitions, the higher the quality of estimations.

In addition, the higher the spatial density of the MP identified and the quality of the dataset, the lower the probability of phase unwrapping errors.

The accuracy of the estimated displacement rate for each MP is described through its standard deviation value parameter (V_STDEV). The standard deviation measures the dispersion of a set of measurements around their mean value, providing indication on their precision. A low standard deviation value indicates that the measurements tend to be very close to the mean, whereas high standard deviation indicates that the data are spread out over a large range of values. Given the standard deviation (σ), under the assumption that the noise on the measurements is normally distributed (or Gaussian), 95% of the values tend to be included in a ±2σ range around the average value.

Considering a dataset of at least 30 scenes covering a 2-year period, a MP located less than 1 km away from the REF had a typical standard deviation value lower than 1 mm/year. The single displacement value precision is on average within ± 5 mm (Table 1). Average precision for single measurement in a time series is not statistically evaluated but derived from validation against ground truth.

Displacement (LOS)	Standard deviation of the average displacement rate	Standard deviation of a single measurement
Accuracy	< 1 mm/yr	< 5 mm

Table 1. Typical values of standard deviation for a MP less than 1 km from the REF using a dataset of at least 30 scenes covering a 2-year period.

SqueeSAR® measurements are also provided with another precision parameter, the error bar (STD_DEF). It is an index that measures how well an analytical model fits an estimated time series. The choice of the appropriate model is done automatically applying a sophisticated Model Order Selection consider several factors: the number of processed images, the time interval between the first and last image and possible gaps in the acquisitions (e.g., sporadic or regular intervals without acquisitions). The better the dataset quality, the more accurate the choice of the model.

An error bar is provided for each MP, in mm, stating the standard deviation of its time series compared to the model. The lower the error bar value, the lower the residual is after fitting the analytical model on the time series, indicating a correct model selection of the deformation dynamic as well as a low noise on the time series. Being influenced by number of images, dataset time span and motion dynamic, it is not possible to directly compare error bar values between different independent SqueeSAR® processing.

2.4. Phase unwrapping and fast movements

As already mentioned, the precision of the measurements depends on performing a correct phase unwrapping. In a case of rapid deformation (construction works) affecting single isolated targets, the phase unwrapping can be affected by an equivocation of the phase.

Figure 4 illustrates a scheme of the equivocation phenomena. The grey solid represents a radar system acquisition target. The target is represented at an initial R_0 distance (in blue), while in red there are three possible cases shifted to R_0 by different entities. Without prior information, the system is not able to estimate the correct number of wavelengths ($n\lambda$) which occurred therefore, all three cases will have equivalent ΔR shift measurement.

More precisely, it is needed to measure the displacement and the direction of motion. This means that theoretically on a single isolated radar target, only displacement below half a wavelength will be correctly detected. A greater displacement may be misinterpreted. In extreme cases, if the target moved exactly half a wavelength between two acquisitions the target would be considered perfectly stable.

These theoretical limits refer to fast movements affecting single isolated radar targets. Measurement ambiguities can be resolved in cases the movement is spatially correlated and the MP density is adequate.

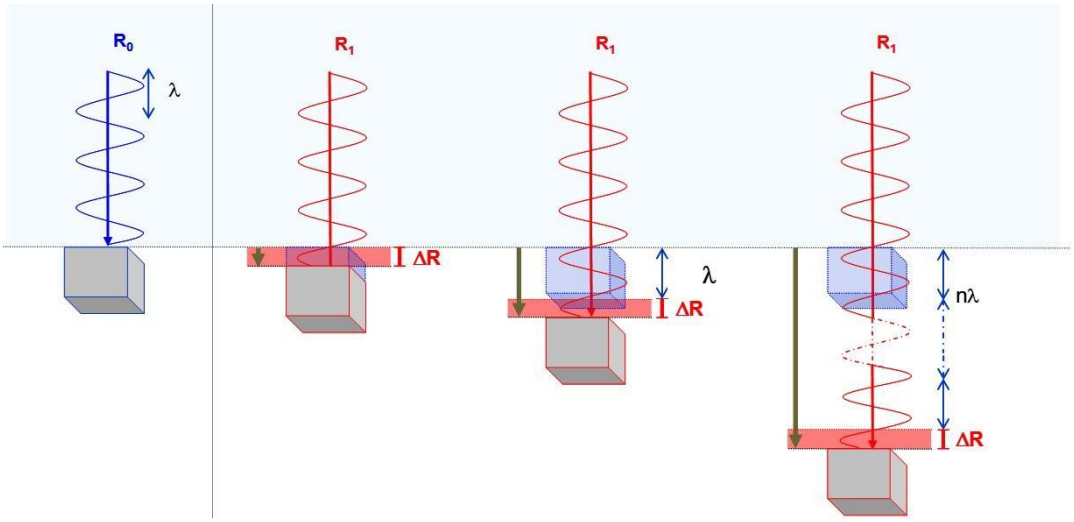

Figure 4. Schematic of a sinusoidal phase of the electromagnetic wave incident on a moving target (grey solid). Without prior information, it is not possible to estimate the correct number of wavelength (në) which occur and in all three cases an equivalent ΔR shift is measured.

Figure 5 shows a schematic of a spatially correlated subsidence phenomenon. When the radar targets density is adequate, a correct phase unwrapping can be operated and a total displacement higher than the λ/4 limit can be measured. In a case where the radar target distribution is not adequate, an incorrect phase unwrapping can cause an underestimation of the displacement which occurred.

The temporal distribution of the acquisitions impacts the phase unwrapping correctness: the higher the acquisition frequency, the higher the ability to correctly unwrap and describe fast movements.

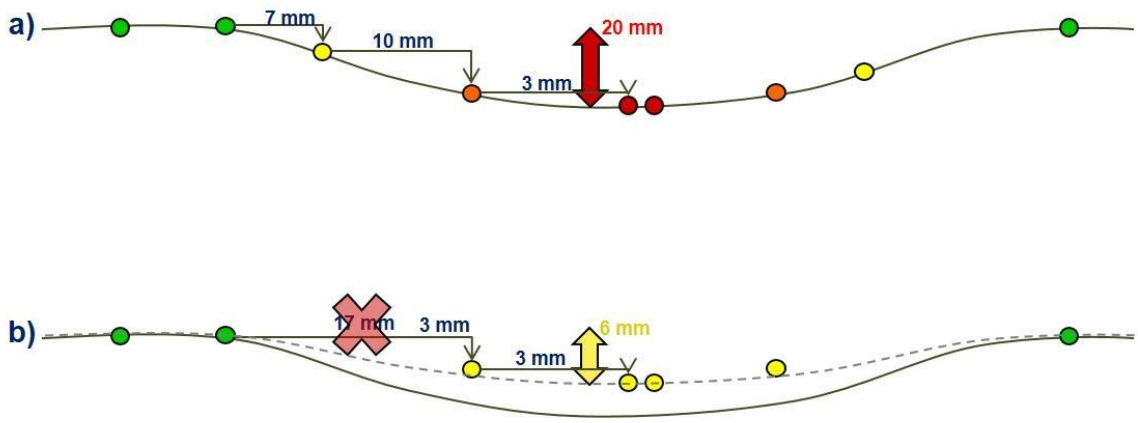

Figure 5. Schematic of a spatially correlated subsidence phenomena. The MP are colour-coded accordingly to the displacement measured. Considering a C-band satellite, a total displacement of 20 mm (higher than the λ/4 limit of 14 mm) can be measured when the MP are well distributed along the subsiding profile (a). When the MP distribution is not adequate, an underestimation of the real displacement occurs (b).

2.5. Geolocation accuracy

Since all InSAR measurements are relative to the REF, the absolute accuracy of the MP location depends on the location of the selected REF for the analysis. In general, InSAR data geocoding is refined using a priori information (e.g., an ortho-photo of the AOI over which InSAR vector data is overlain or a set of ground control points). However, the absolute location of the REF with respect to the International Terrestrial Reference Frame (ITRF) can be verified only using an independent GNSS (Global Navigation Satellite System).

Nevertheless, in most applications the relative accuracy of the target's coordinates (i.e., measurement of how well the vector between two points is measured) is much more important than absolute accuracy, since any systematic shift can be dealt with quite easily and these shifts do not typically compromise data interpretation.

Table 2 reports the typical accuracy values associated to the UTM coordinates of MP at mid-latitudes. Figure 6 shows the typical precision values associated to satellites commonly used in operational SqueeSAR® processing.

Direction	C-band SNT [m]	X-band TSX [m]
North	± 8	± 1
East	± 12	± 3
Vertical (elevation)	±8	± 1.5

Table 2: Typical precision values (1 sigma) associated to the UTM coordinates of a MP at mid-latitudes. Values are referred to a MP less than 1 km from the REF and a dataset of at least 30 SAR scenes.

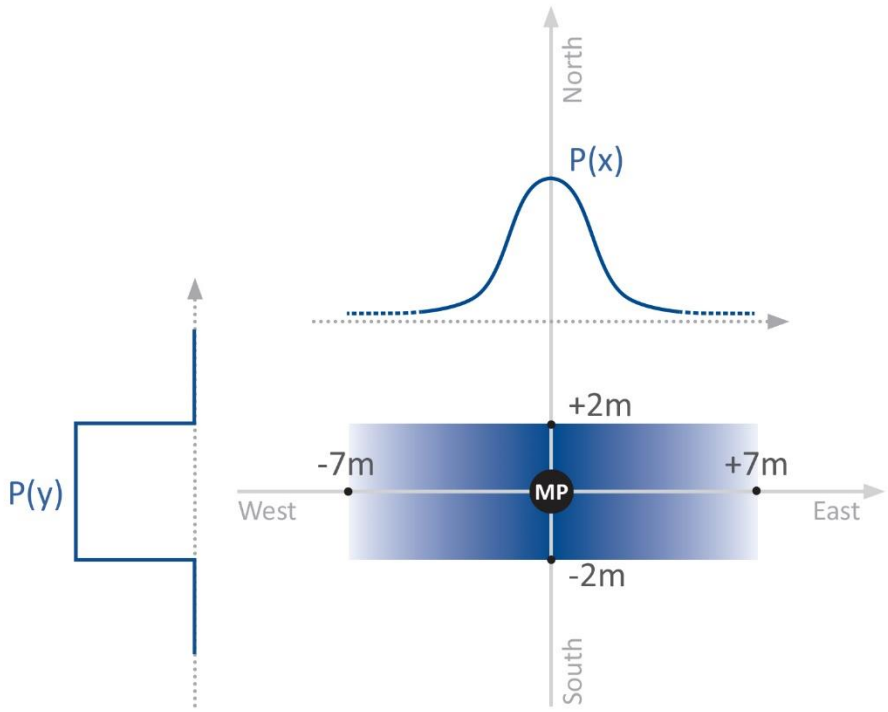

Figure 6: Typical precision values associated to C-band ERS and ENVI data. Values are referred to a MP less than 1 km from the REF and a dataset of at least 30 SAR scenes.

An estimation of the geolocation accuracy is provided with the SqueeSAR® results with the parameter GEO_STDEV. This parameter is derived from the spatial resolution of the SAR image and the H_STDEV parameter (accuracy of the estimated height of the MP).

3. SAR Data

The historical radar data available over the AOI consists of medium and high-resolution images acquired by the SNT and TSX satellites from descending orbit (satellite travelling from north to south and imaging to the west; Table 3). The SNT mission is operated by the European Space Agency (ESA) and is composed of a constellation of two satellites, Sentinel-1A and Sentinel-1B, which share the same orbit and acquire in C-band (wavelength = 5.66 cm) at a ground resolution of 20 m x 5 m. The TSX mission is operated by the German Space Agency (DLR) and owned by Airbus. The TSX satellite is closely followed by its twin TanDEM-X on the same orbit, and they are backed up by the Spanish satellite PAZ. They acquire in X-band (wavelength = 3.10 cm) at a ground resolution of 3 m x 3 m.

The 349 SNT images cover the period from November 18th, 2014, to October 12th, 2021, with 6-day revisit frequency (Table 3). The 53 TSX images cover the period from June 13th, 2014, to March 23rd, 2016, with a 11-day revisit frequency (Table 3).

Satellite	Pixel Resolution	Orbit Geometry	Track	LOS Angle (θ)	# Images	Date Range
Sentinel-1	20 m x 5 m	Descending	110	34.84°	349	18 Nov. 2014 – 12 Oct. 2021
TerraSAR-X	3 m x 3 m	Descending	48	20.86°	53	13 Jun. 2014 – 23 March 2016

Table 3: Satellite acquisition parameters and image acquisition information.

The temporal distribution of SNT (descending geometry in purple) and TSX (descending geometry in blue) images processed is shown in Figure 7.

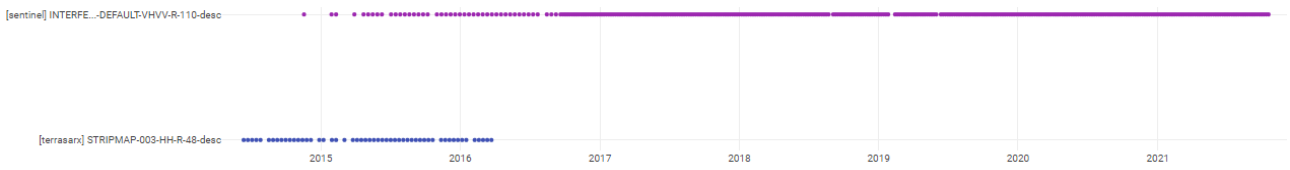

Figure 7: Temporal distribution of SNT (purple) and TSX (blue) images processed over the AOI.

Finally, the characteristics of the image acquisition for SNT and TSX satellites are given in the Figure 8 and the Figure 9 (the θ angle represents the inclination to the vertical and the δ angle represents the inclination the North-South axis).

Satellite info

Satellite	Wavelength	Satellite geometry	Sensor mode	Satellite track
SNT	5.55 cm	DESCENDING	IW	110

Acquisition geometry

Line of sight angle	**ɵ:**	34.84°	**δ:**	9.68°		
Line of sight versors	**V:**	0.821	**N:**	-0.096	**E:**	0.563

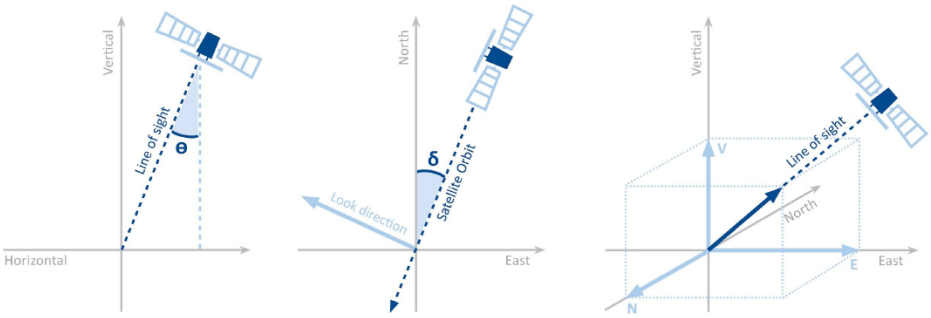

Figure 8: Acquisition geometry in descending mode for the SNT images used for the SqueeSAR® analysis.

Satellite info

Satellite	Wavelength	Satellite geometry	Sensor mode	Satellite track
TSX	3.11 cm	DESCENDING	SM003	48

Acquisition geometry

Line of sight angle	**ɵ:**	20.86°	**δ:**	11.3°		
Line of sight versors	**V:**	0.934	**N:**	-0.07	**E:**	0.349

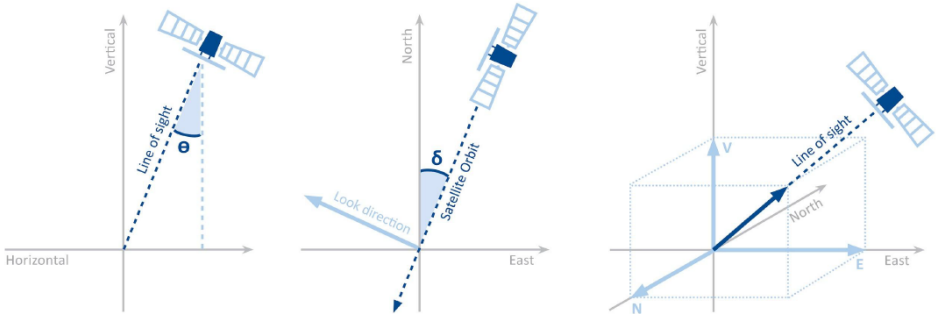

Figure 9: Acquisition geometry in descending mode for the TSX images used for the SqueeSAR® analysis.

Figure 10 represents the footprints of the SNT and TSX images in purple and blue, respectively. The AOI is entirely included in both.

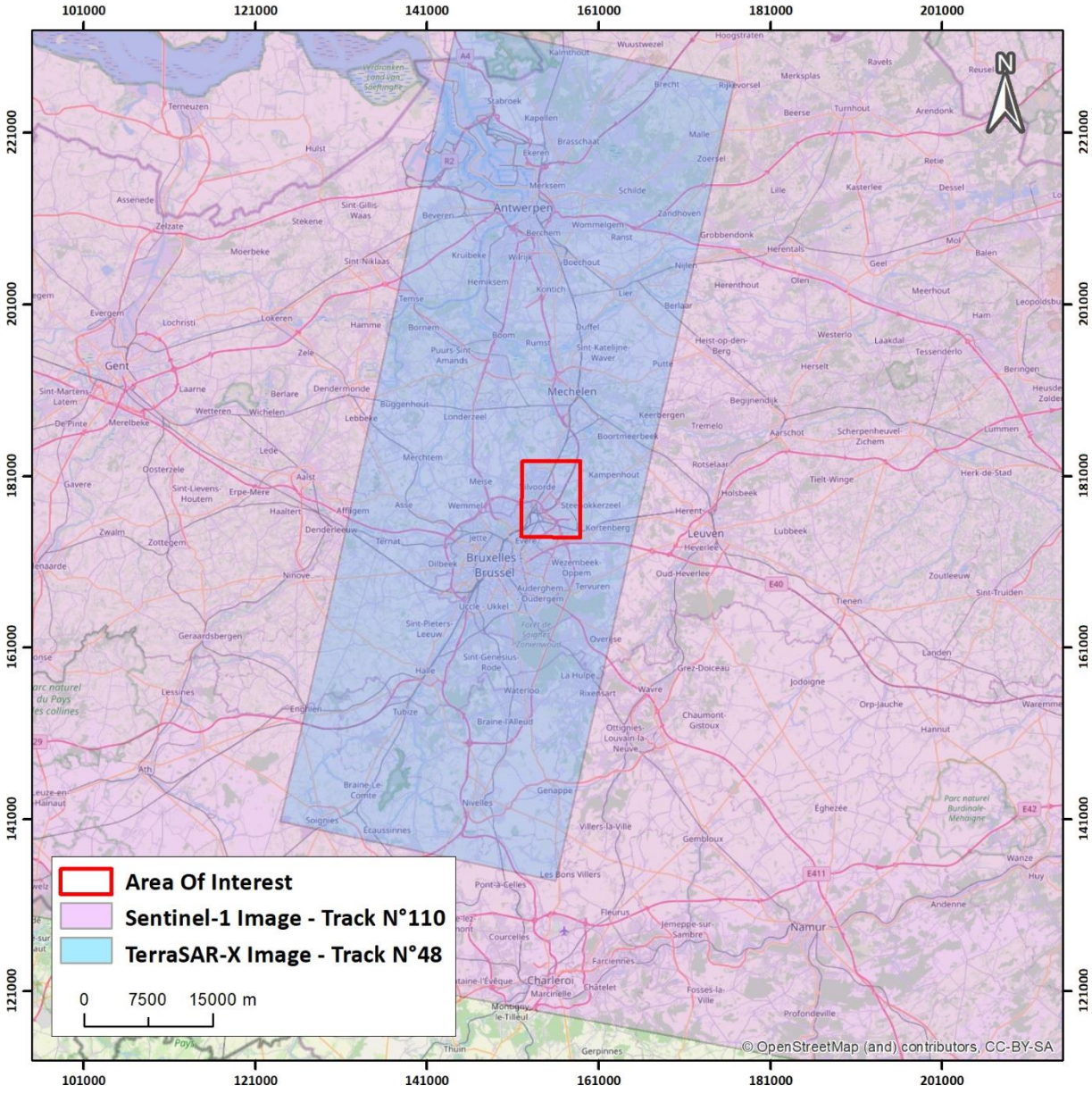

Figure 10. Area Of Interest (in red) of the POC, the footprints of SNT and TSX images are represented in purple and blue, respectively.

4. Results

4.1. Reference Point

The REF for both analyses are located in the north part of the AOI, in the municipality of Vilvoorde. The information related to the SNT and TSX SqueeSAR® analysis are reported in the Table 4 and the Table 5, respectively.

Code	Geographic coordinates (°)		Plane coordinates Lambert 72 (m)	
	Longitude	Latitude	East	North
B4SSDPR	4.4502415	50.923794	155 729.46	179 278.84

Table 4: REF location for the SNT SqueeSAR® analysis.

Code	Geographic coordinates (°)		Plane coordinates Lambert 72 (m)	
	Longitude	Latitude	East	North
AVCTVES	4.4506696	50.9499496	155 756.32	182 188.52

Table 5: REF location for the TSX SqueeSAR® analysis.

The location REF for both SNT and TSX SqueeSAR® analysis are presented in the Figure 11.

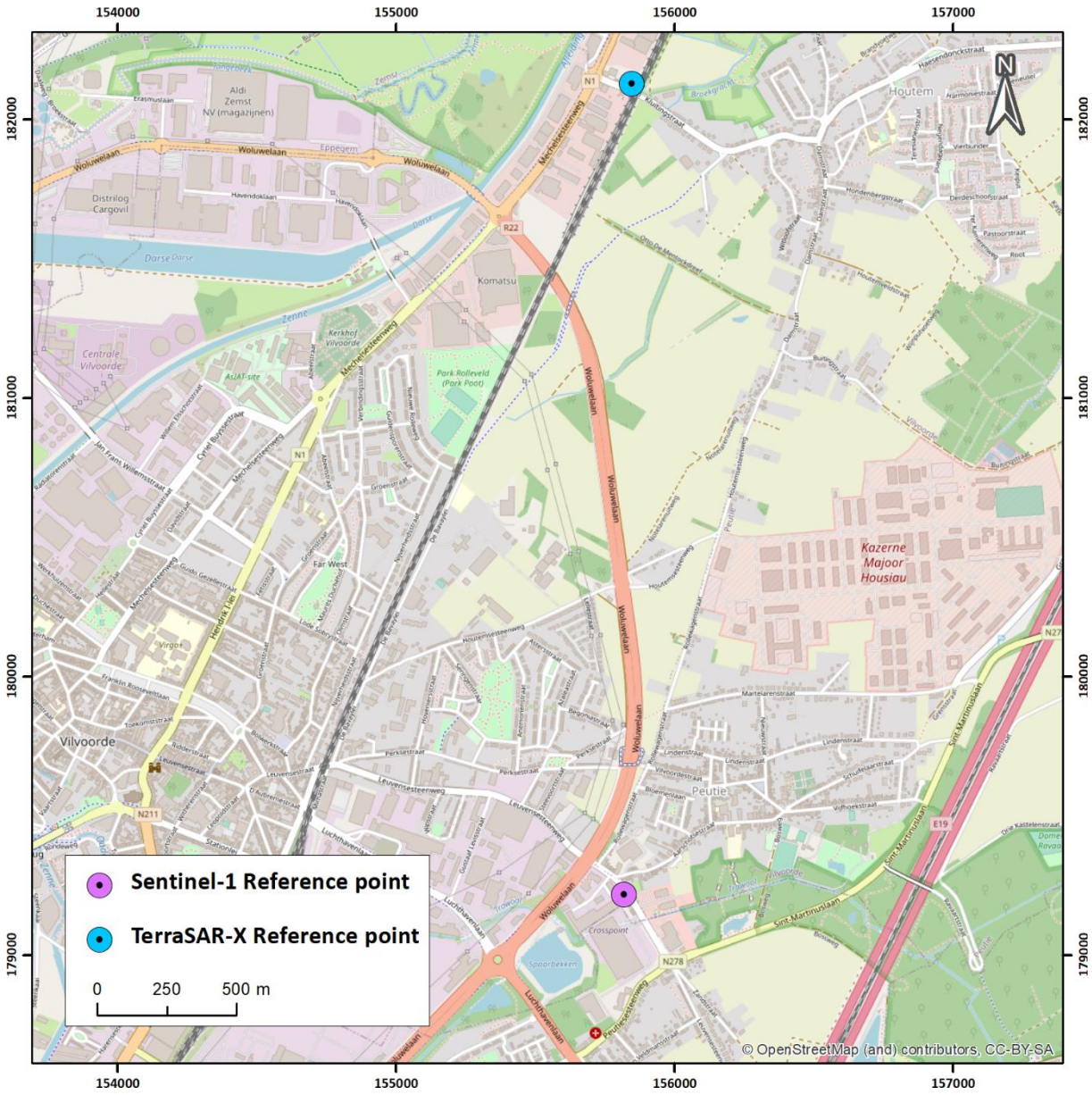

Figure 11. Location of spatial REF points for the SNT (purple) and TSX (blue) SqueeSAR® results, respectively.

4.2. Permanent Scatterers (PS) and Distributed Scatterers (DS)

For the SNT SqueeSAR® analysis, 132 971 MP have been obtained for a spatial density of 2417 MP/km². The statistical repartition of the nature of MP shows a high percentage of PS due to the urban context of the study (Table 6).

Nb. of MP	Type	
	PS	DS
132 971	127 080	5 891
100 %	95.57 %	4.43 %

Table 6: Statistical repartition of MP for the SNT SqueeSAR® analysis.

For the TSX SqueeSAR® analysis, 1 113 221 MP have been obtained for a spatial density of 20 240 MP/km² (roughly 10 times higher than the SNT study). The statistical repartition also shows a high percentage of PS (Table 7).

Nb. of MP	Type	
	PS	DS
1 113 221	1 028 616	84605
100 %	92.40 %	7.60 %

Table 7: Statistical repartition of MP for the TSX SqueeSAR® analysis.

The statistics reported in the Table 6 and the Table 7 show the same behaviour between the SNT and TSX analysis: ~94% of PS and ~6% of DS. Despite the repartition, the TerraSAR-X study shows 10 times more MP than the SNT study.

The Figure 12 and the Figure 13 show the spatial distribution of the PS and DS through the SqueeSAR® analysis, respectively. The spatial distribution is similar between the two studies, with PS are located in urban areas and DS predominantly located in areas with moderate vegetation or agricultural fields.

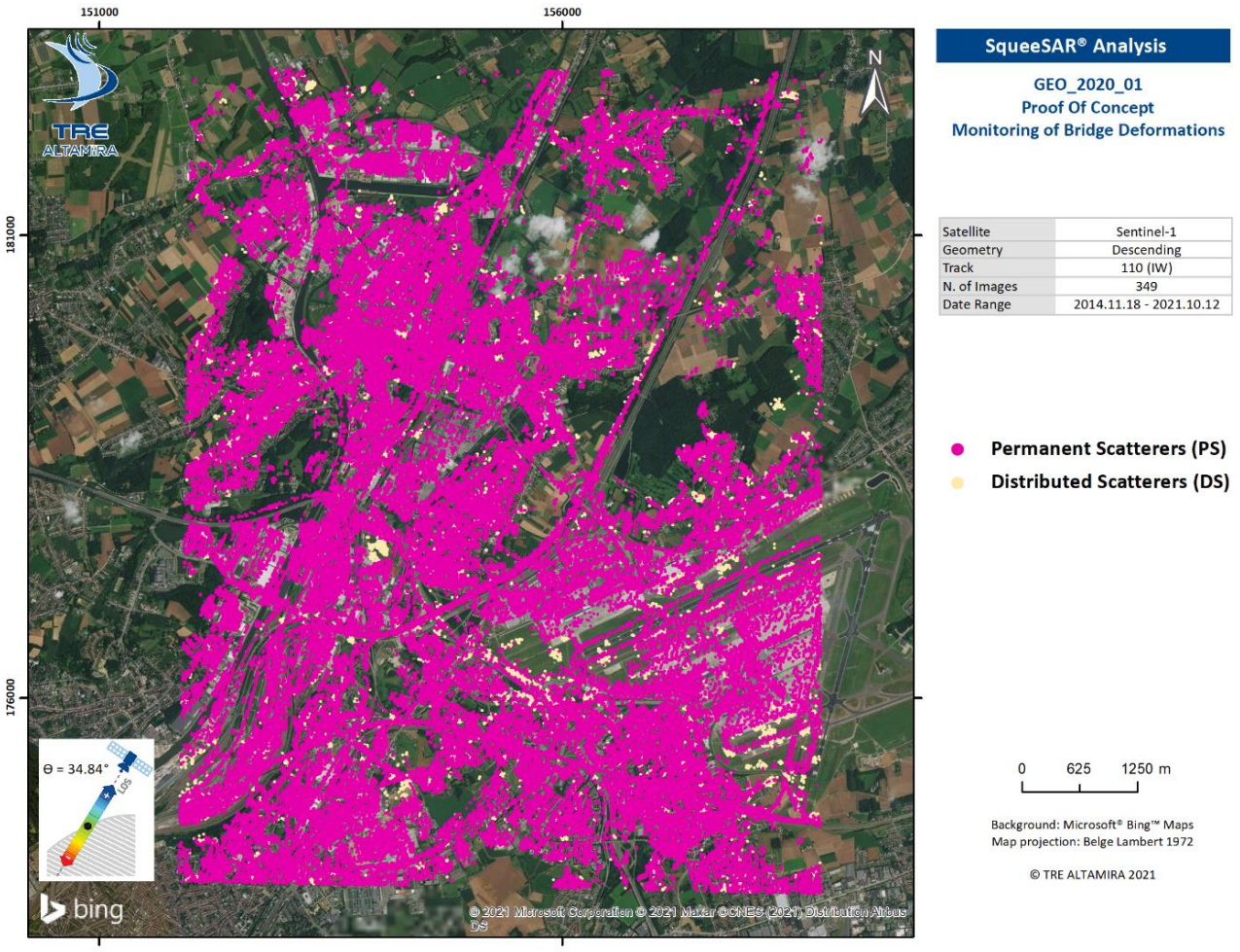

Figure 12. Spatial distribution of the PS and DS through the SNT SqueeSAR® results.

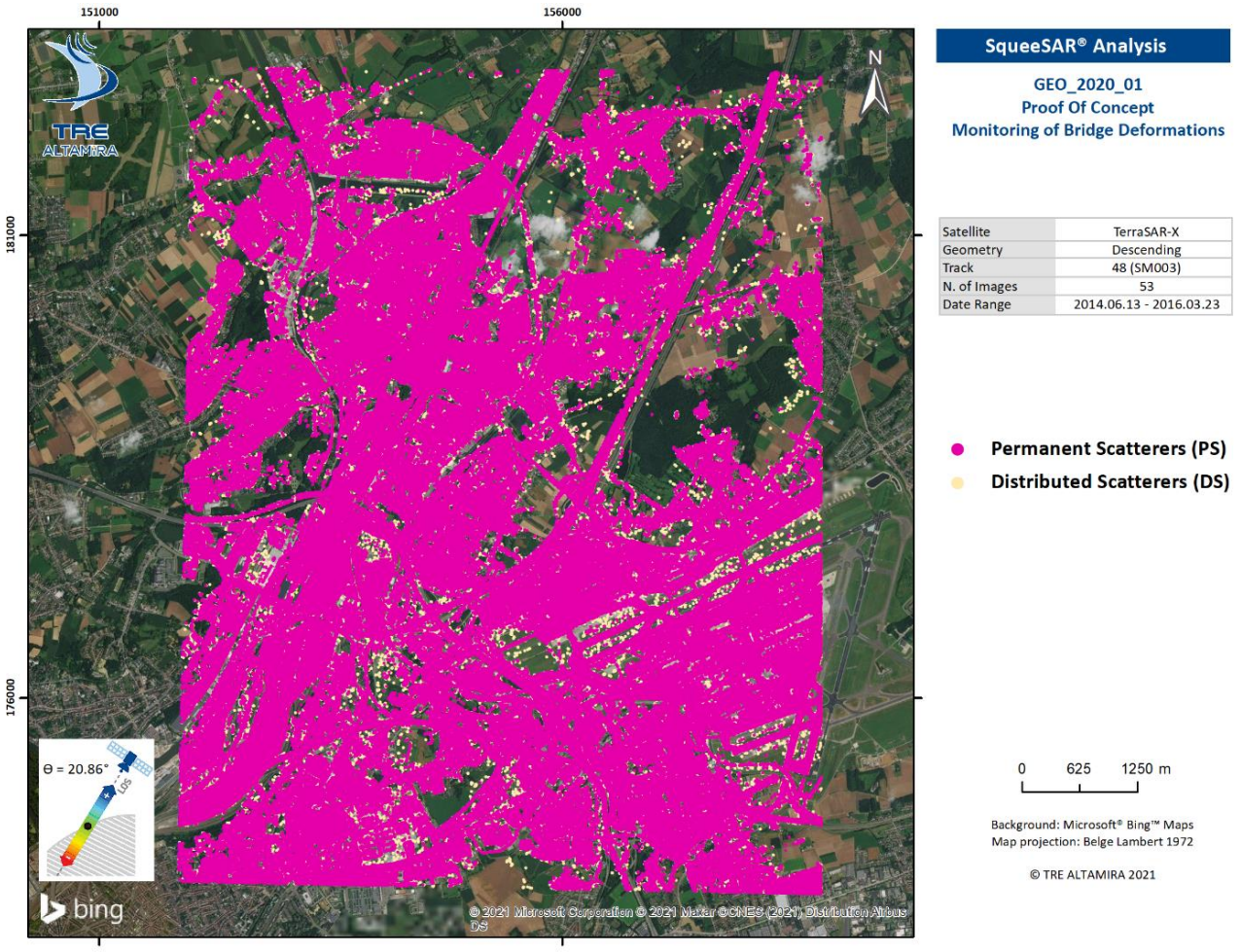

Figure 13. Spatial distribution of the PS and DS through the SNT SqueeSAR® results.

4.3. LOS deformation and deformation rate maps

The LOS deformation measured in millimetres from the SNT descending archive (18 Nov 2014 to 12 Oct 2021) is shown in Figure 14. The deformation rates range from -91 mm to 49 mm with a standard deviation of ± 7.7 mm (Figure 14). Some small-scale deformation areas are observable.

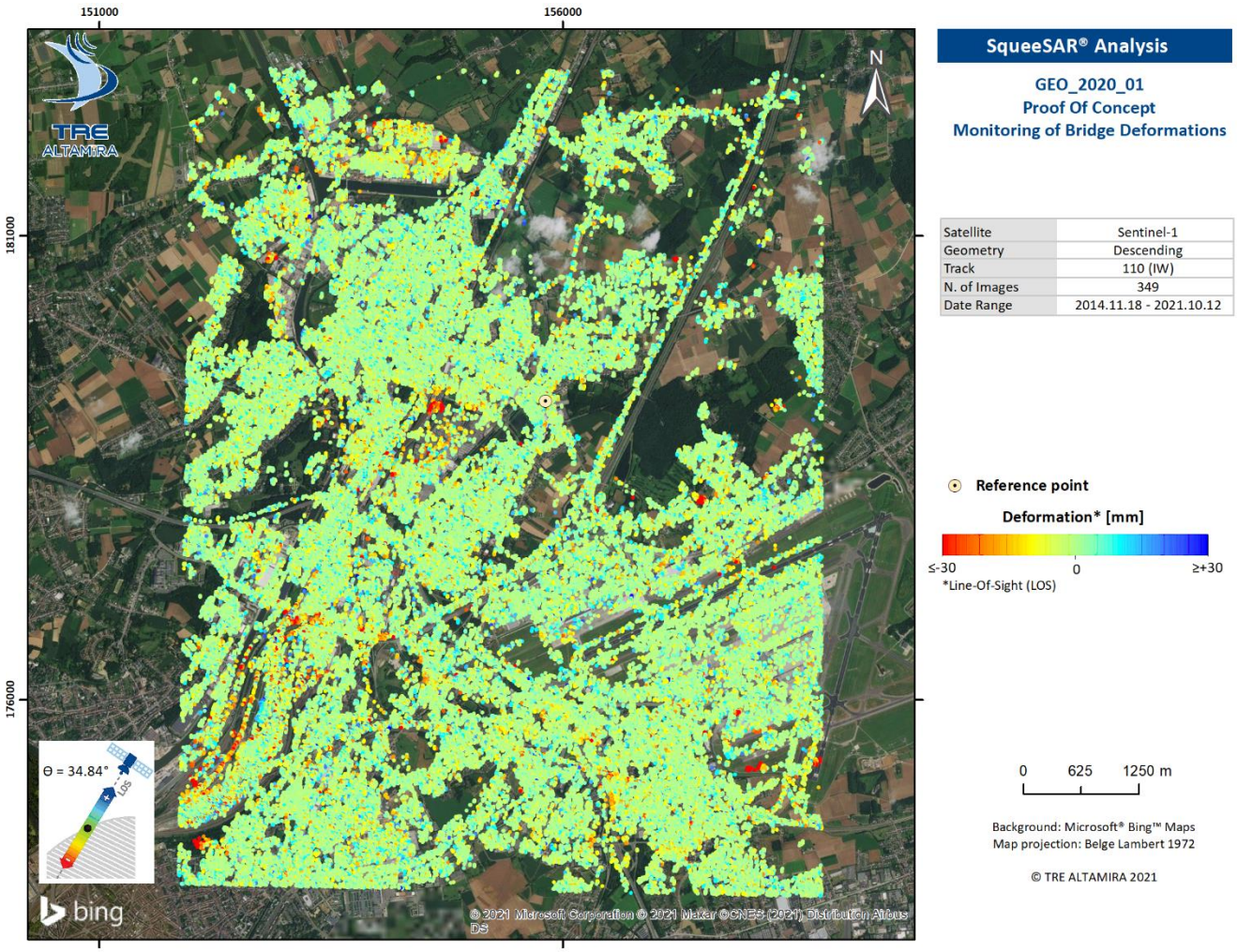

Figure 14: LOS deformation from the descending geometry of SNT SqueeSAR® analysis.

The LOS deformation rates measured in millimetres per year from the SNT descending archive (18 Nov 2014 to 12 Oct 2021) is shown in Figure 15. The deformation rates range from -12 mm/yr to 6 mm/yr with a standard deviation of ± 0.9 mm/yr (Figure 15). The same small-scale deformation areas are noticeable.

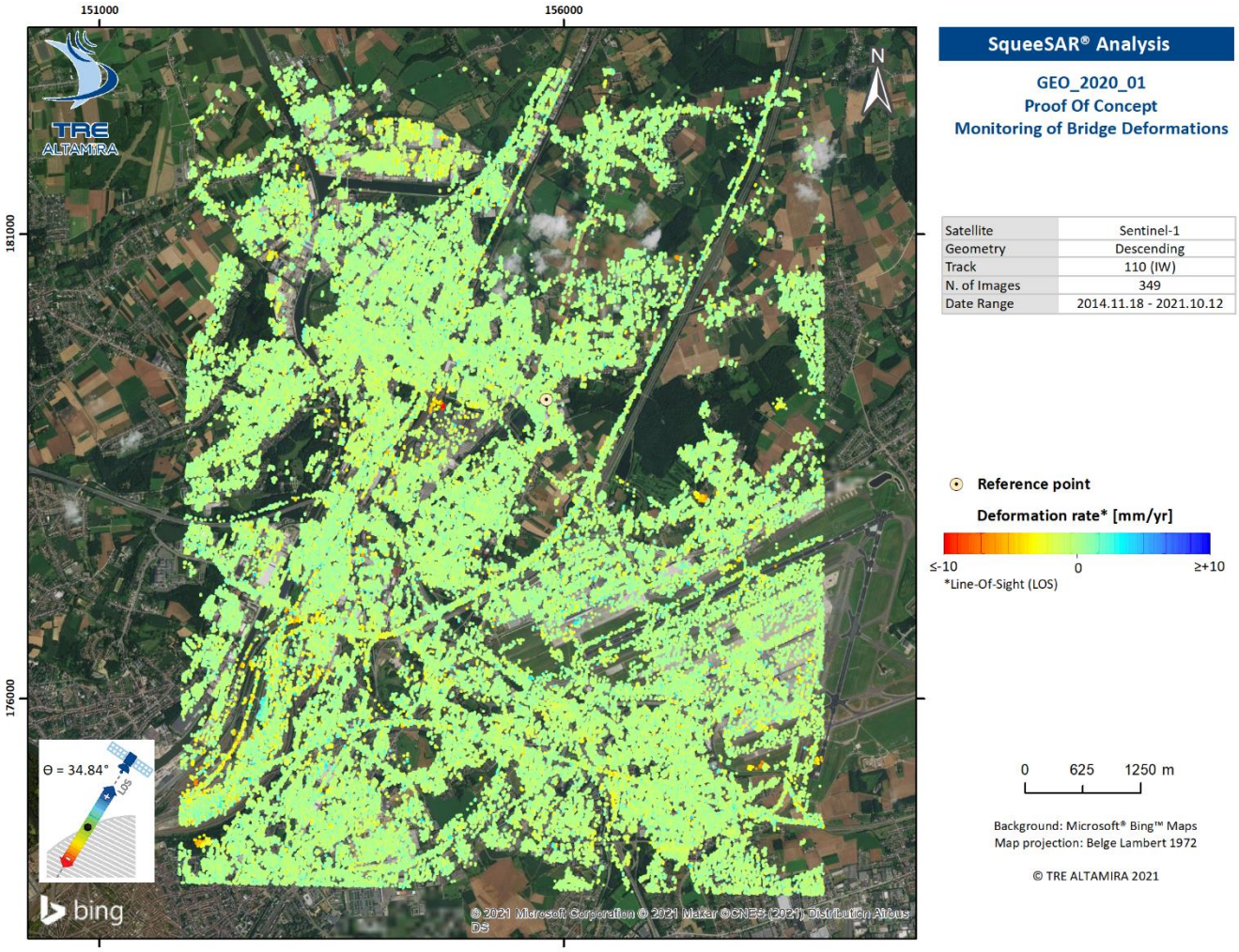

Figure 15: LOS deformation rates from the descending geometry of SNT SqueeSAR® analysis.

The LOS deformation measured in millimetres per year from the TSX descending archive (13 Jun 2014 to 23 Mar 2016) is shown in Figure 16. The deformation rates range from -60 mm to 27 mm with a standard deviation of ± 3.8 mm (Figure 16). Some small-scale deformation areas are observable at the same locations than the SNT SqueeSAR® analysis (Figure 14).

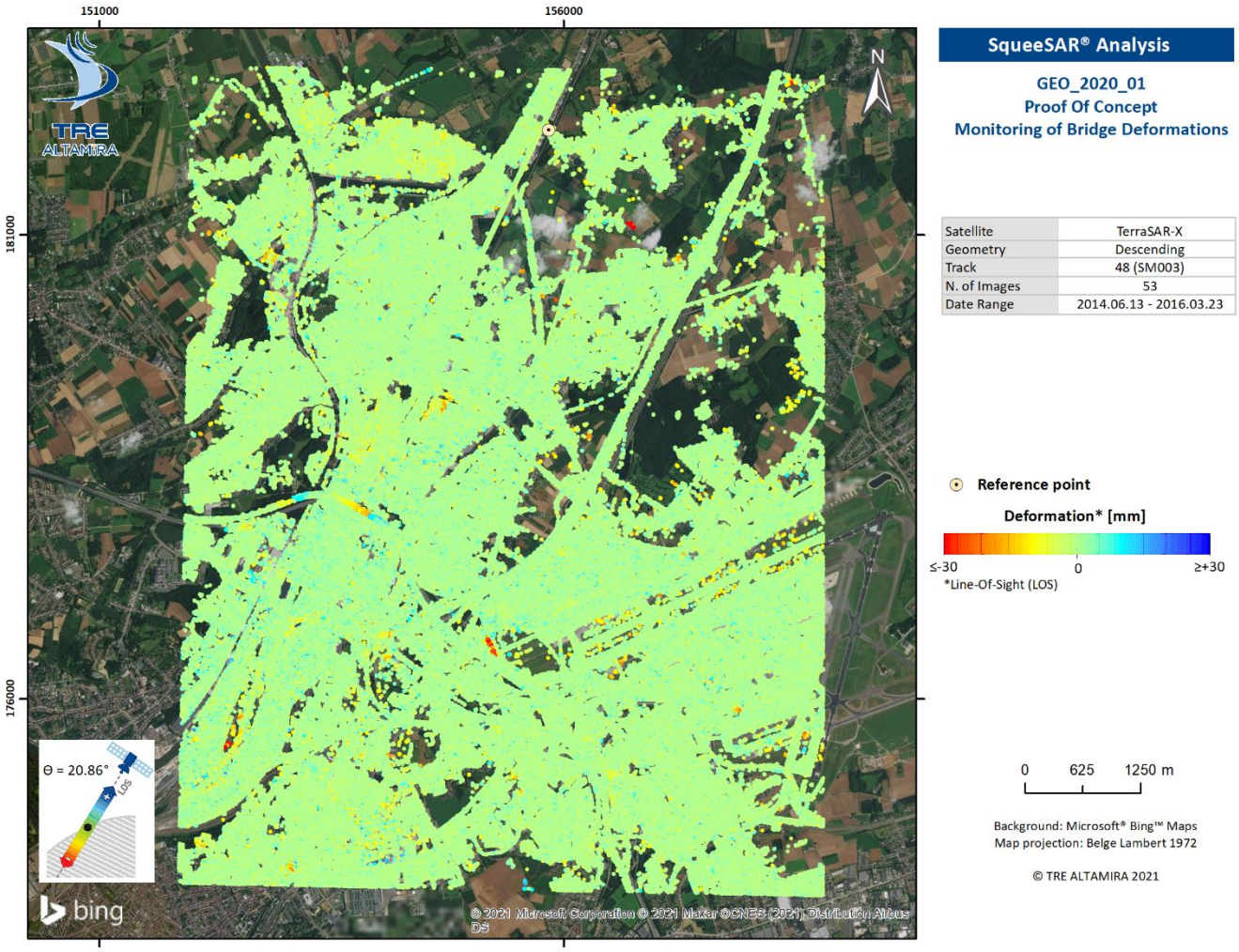

Figure 16: LOS deformation from the descending geometry of TSX SqueeSAR® analysis.

The LOS deformation rates measured in millimetres per year from the TSX descending archive (13 Jun 2014 to 23 Mar 2016) is shown in Figure 17. The deformation rates range from -31 mm/yr to 11 mm/yr with a standard deviation of ± 1.5 mm/yr (Figure 17). Small-scale deformation areas can be seen at the same locations than the SNT SqueeSAR® analysis (Figure 15).

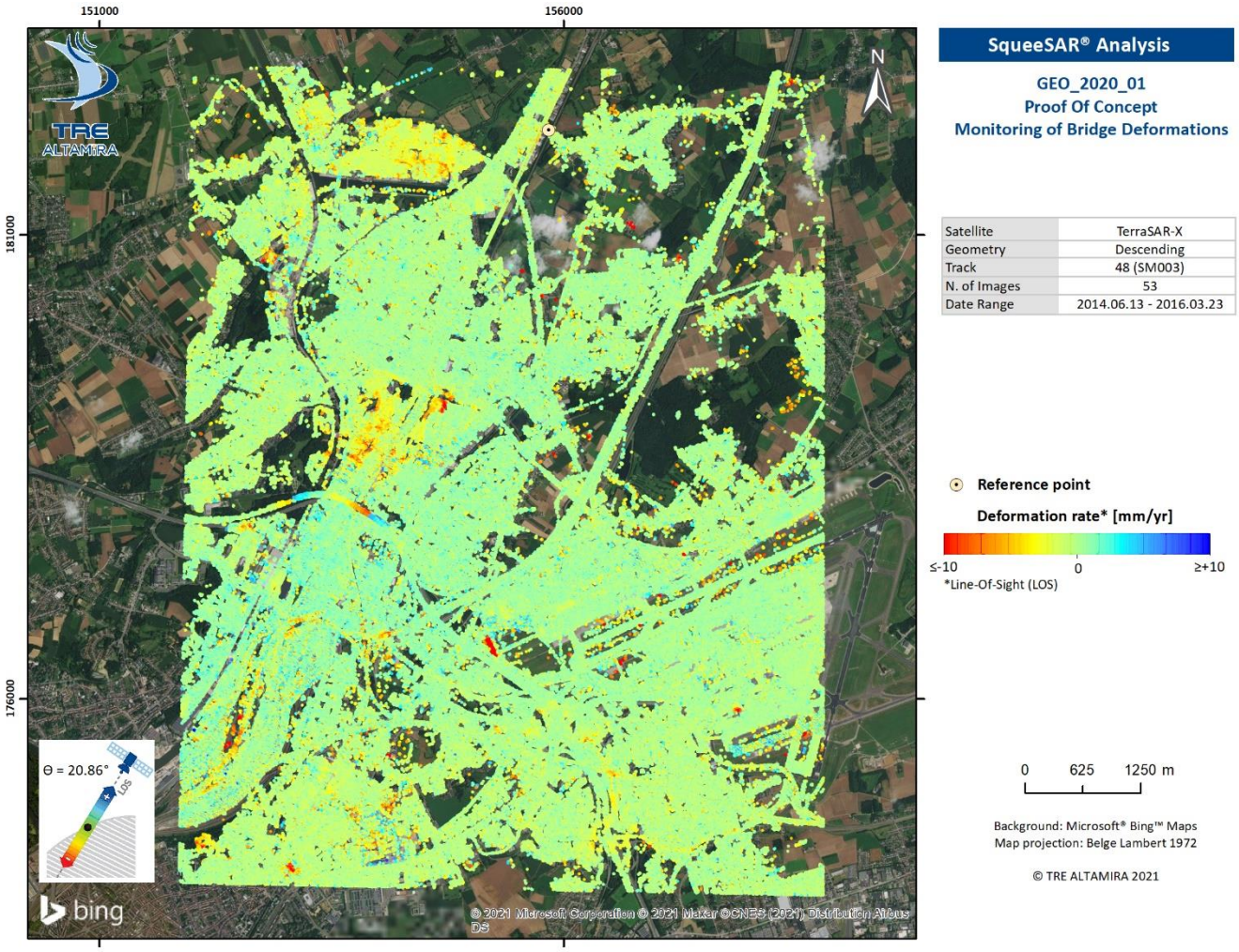

Figure 17: LOS deformation rates from the descending geometry of TSX SqueeSAR® analysis.

4.4. Seasonal Amplitude maps

The seasonal (annual) amplitude in millimetres from the SNT descending archive is shown in Figure 18. The seasonal amplitude reaches a maximum of 6.7 mm (Figure 18). The highest seasonal amplitude observed over a bridge is on the Viaduct van Vilvoorde with a value of 6.7 mm located to the west of the AOI.

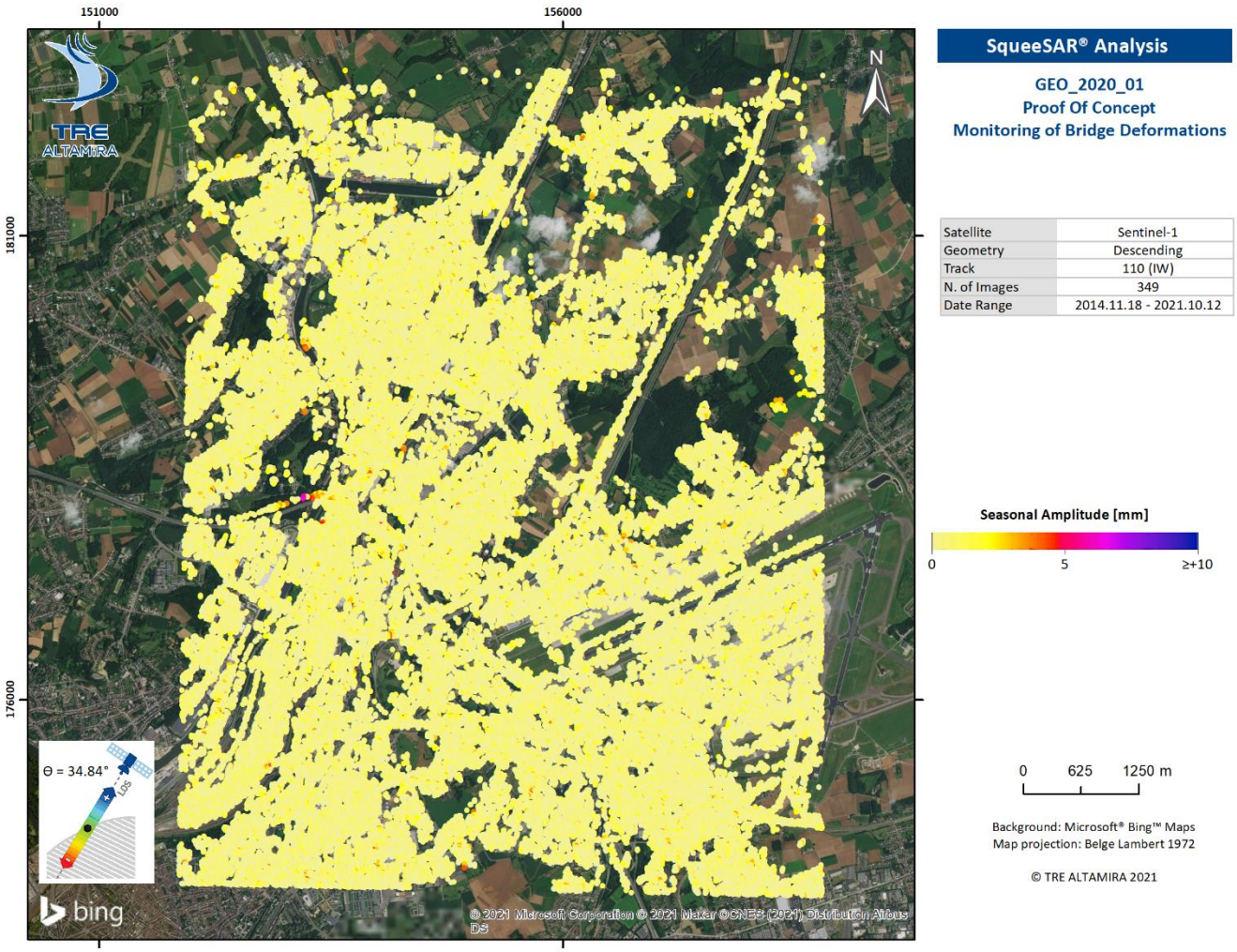

Figure 18: Seasonal (annual) amplitude from the descending geometry of SNT SqueeSAR® analysis.

The seasonal (annual) amplitude in millimetres from the TSX descending archive is shown in Figure 19. The seasonal amplitude reaches a maximum of 18.9 mm (Figure 19). The highest seasonal amplitude observed over a bridge is on the Viaduct van Vilvoorde with a value of 18.9 mm located to the west of the AOI.

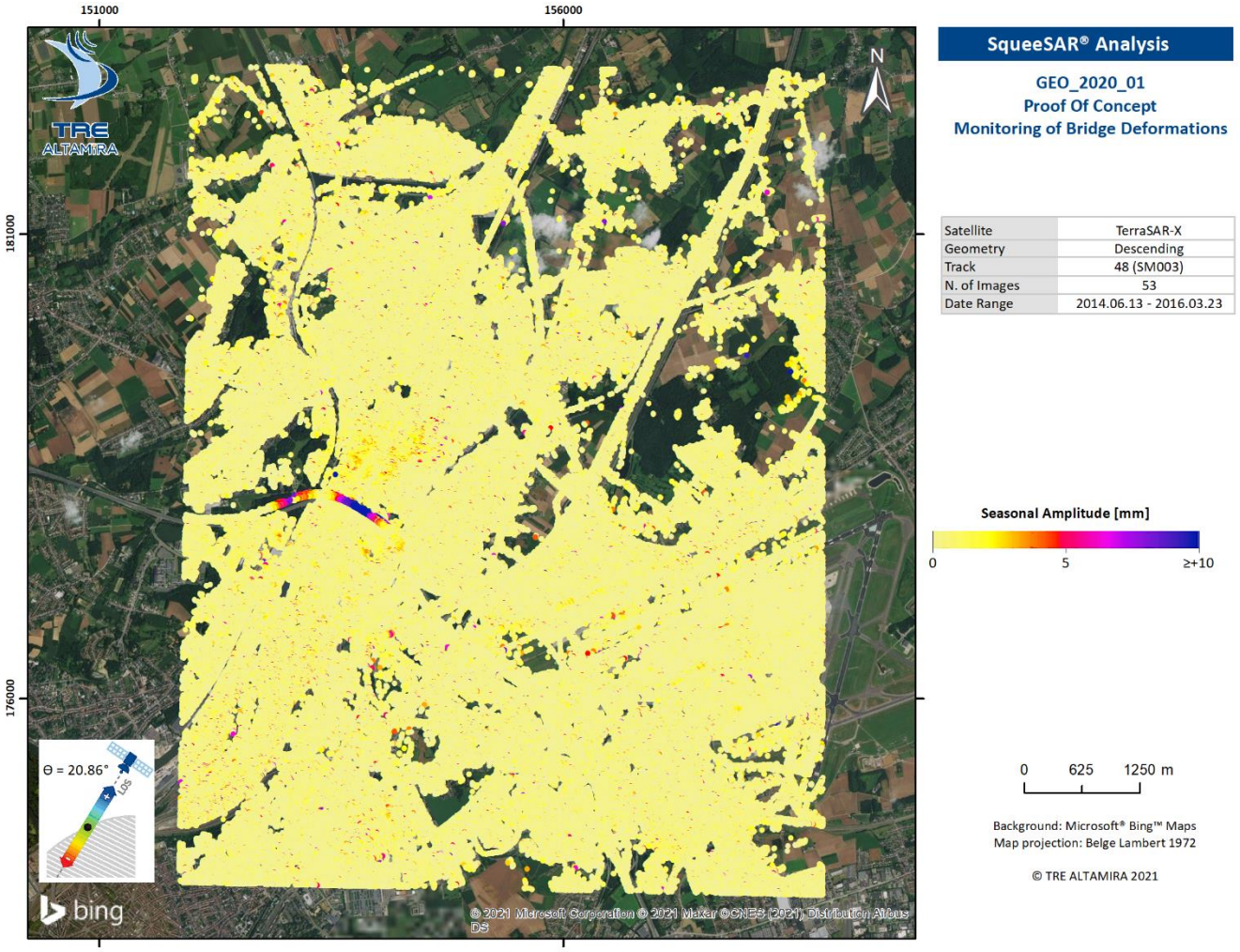

Figure 19: Seasonal (annual) amplitude from the descending geometry of TSX SqueeSAR® analysis.

4.5. Observation

4.5.1. Time series analysis

SqueeSAR® results allows to analyse the temporal behaviour of each MP by displaying their time series. The Figure 20 shows an example of the temporal behaviour of 3 MPs over the Viaduct van Vilvoorde from the TSX study.

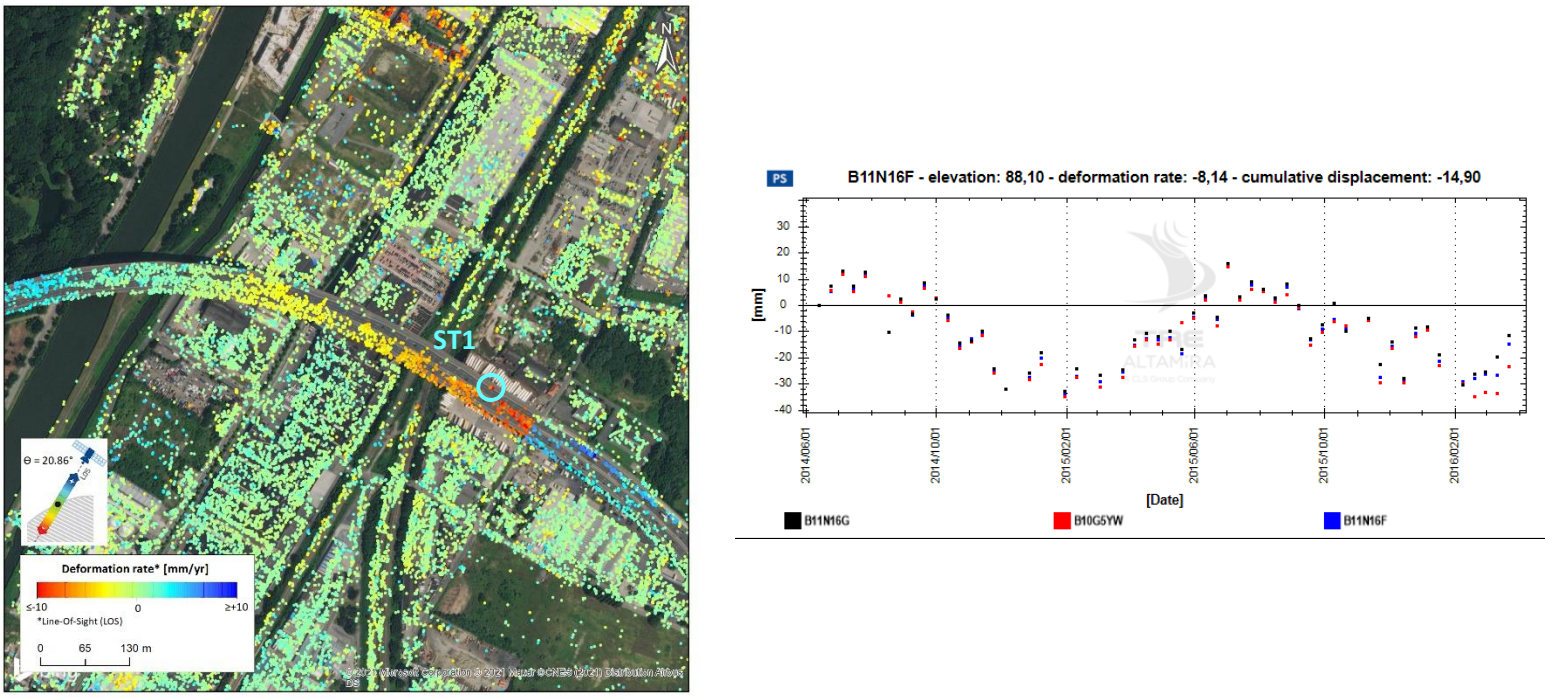

Figure 20: Left: TSX SqueeSAR® velocities (mm/yr) over the Viaduc van Vilvoorde. Right: Time series of the MPs in sector ST1.

4.5.2. Deformation profile analysis

SqueeSAR® results allows to analyse the spatiotemporal behaviour of all the MP over a single bridge with a deformation profile. The Figure 21 shows an example of the spatiotemporal behaviour of all MPs over the Gouletbrug from the TSX study. The deformation profile has a node every 10 m with cells with 10 m long and 20 m wide.

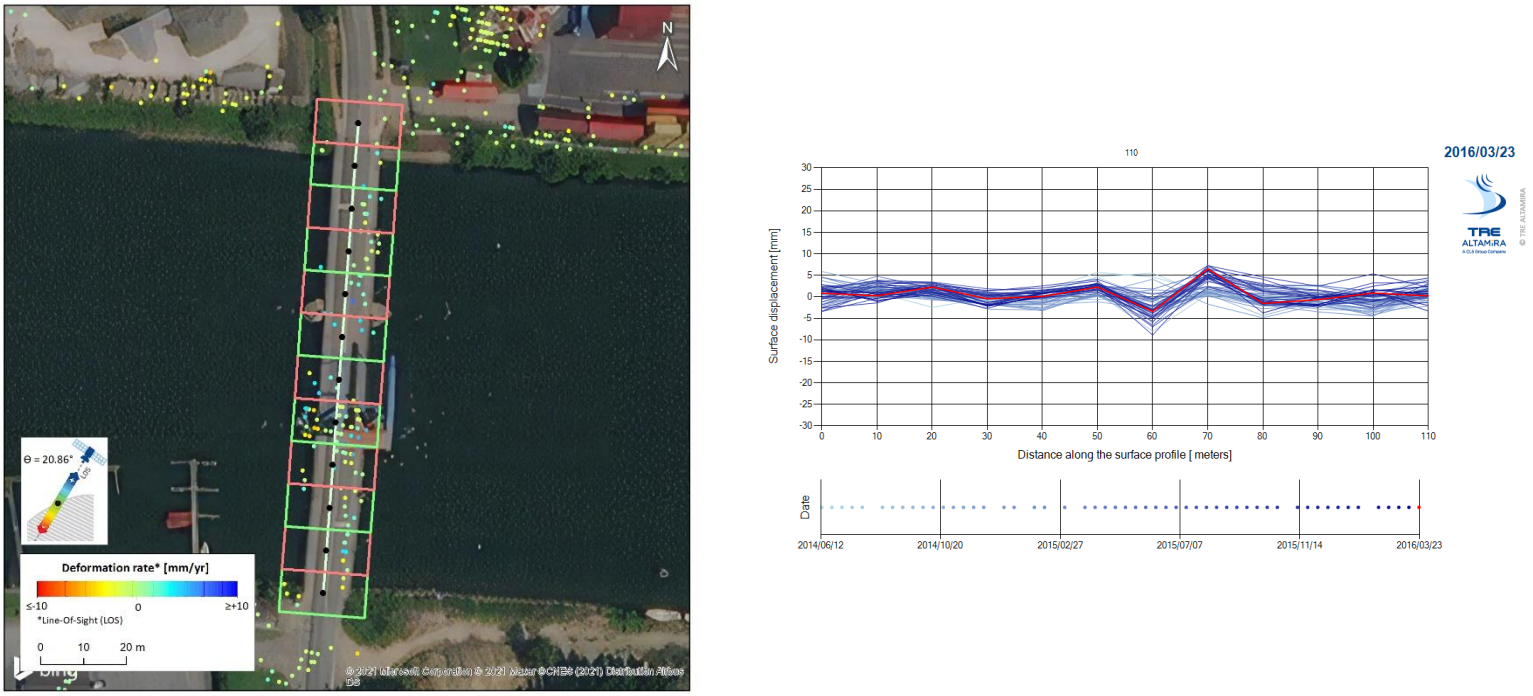

Figure 21: Left: TSX SqueeSAR® velocities (mm/yr) over the Gouletbrug. Right: Associated deformation profile.

The number of nodes, length, and width of each cell of the deformation profile are adjustable to the client's needs, it can also be carried out on the flight on the TREmaps® web visualiser.

5. Additional requirements

5.1. Surroundings

The results of the InSAR analysis in the surroundings of the bridge must be available. It is clear which points are located on the bridge and which are not located on the bridge, and for which points this is uncertain. This classification will help to differentiate which part of the deformation is on the bridge and which deformation is located in the surroundings of the bridge.

TRE ALTAMIRA has developed a methodology using the a priori information of the bridge boundaries and the estimated individual parameters of absolute HEIGHT and DEM correction from the SqueeSAR® processing for each MP, and based in the latter, the overall statistics of the average height of each bridge and the standard deviation of the height of each bridge. The Table 8 present explanations related to each value of the SURR_CLASS field.

Surrounding Classification "SURR_CLASS"	Class Definition
0	Points that are externally of the bridge, or points that are on the ground or with an inconclusive height in comparison with the average heigh of the bridge
1	Points that there is uncertainty whether they are in the bridge deck or in the ground or other external structures that are within the bridge boundary or very close surroundings (6 meters as maximum)
2	Points that are on the bridge deck or structures with similar height, points that are within the bridge boundary or very close surroundings and have similar height to the average height of the bridge

Table 8: Satellite acquisition parameters and image acquisition information.

Geolocation inaccuracies and corrections of the height may cause minimum misalignments between the bridge edges and some external points that have similar parameters to the bridge points. To tackle this aspect, external points in the limits of the bridge have been considered and classified. The distance taking in consideration the external points has been set up to 6 meters and the criteria has been linked to the same statistics of the reliable points on the bridge.

The Figure 22 presents an example of the MP's heights around the Viaduct von Vilvoorde and the corresponding classification.

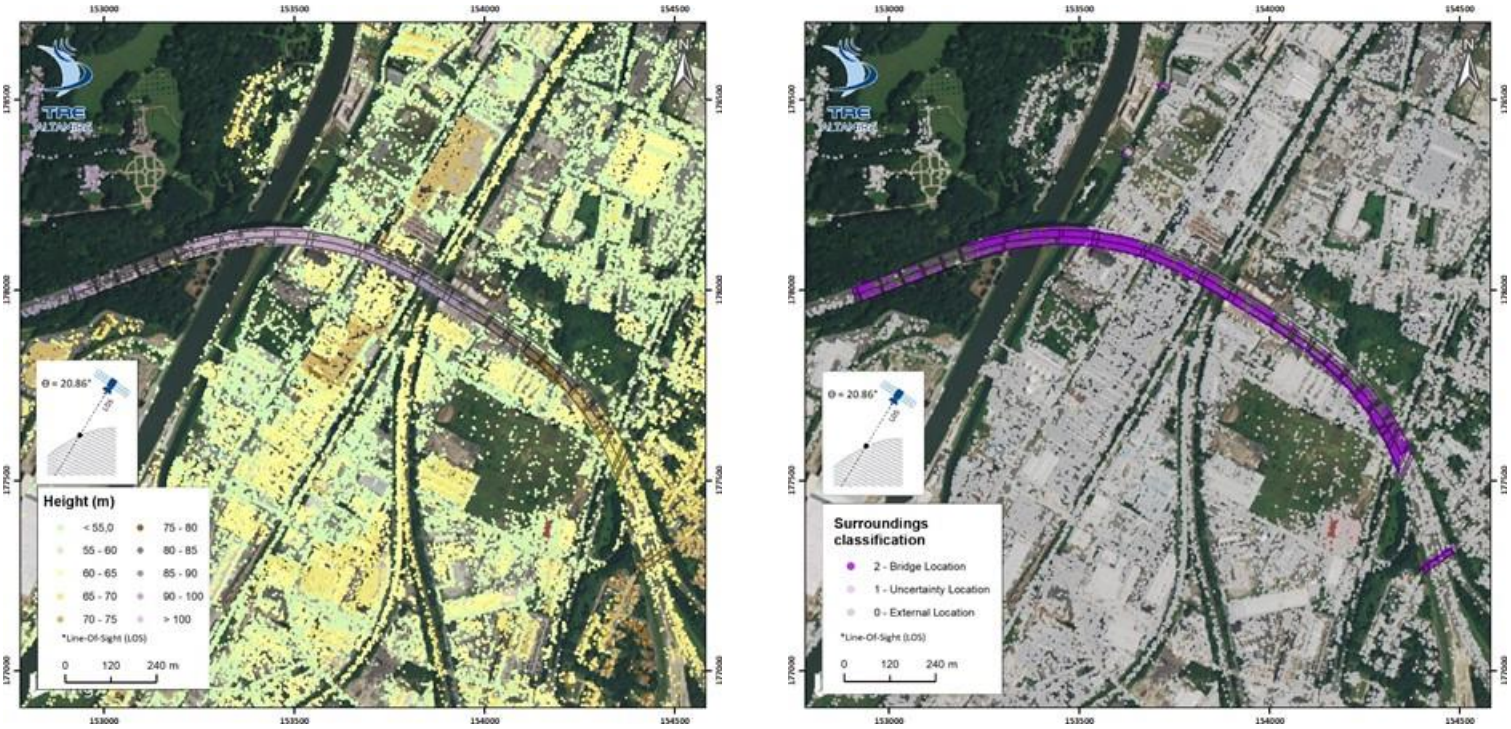

Figure 22. Left: Height of the MP in the vicinity of the Viaduct van Vilvoorde. Right: Classification of the MP in the vicinity of the Viaduct von Vilvoorde.

5.2. Trend Variation maps

The SqueeSAR® algorithm is not forced to use a linear model for the displacement estimation and non-linear or seasonal component (like thermal one) are managed, preserving MPs with such behaviour for further analyses. Trend Variation detection can act as an alert system by flagging any time series exhibiting abnormal motion or trend changes.

The Trend Variation (TV) analysis is performed using a moving window on each time series. The parameters used to trigger alerts would be selected by the Client, however, may be similar to the examples shown below (Figure 23) with the initial parameters:

- Change in rate (ΔV) = 5 mm/yr, Δstep = 5 mm.
- Moving window (Dt) = 90 days.
- To remove single outliers, a spatial consistency threshold will also be applied (clusters of at least 5/6 points within a 100 m radius).

The Figure 23 shows examples of times series that would be flagged for either a change in displacement trend, or for an offset in motion.

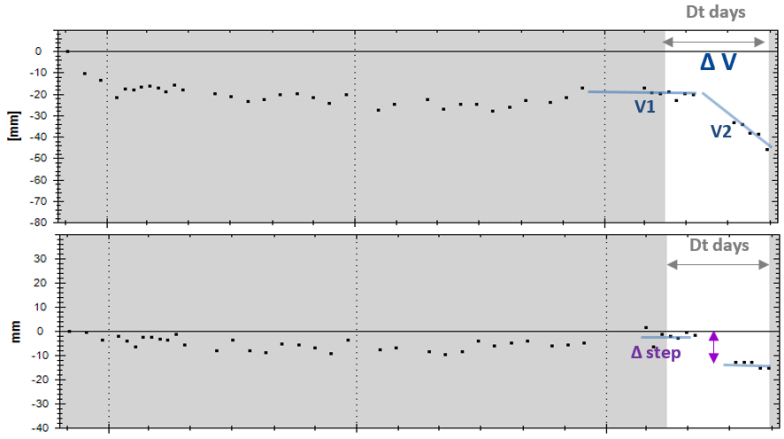

Figure 23: Examples of Trend Variation analysis.

In the scope of the monitoring of bridge deformations, common parameters have been chosen for both SNT and TSX SqueeSAR® analysis:

- Δstep = 5 mm.
- Moving window (Dt) = 60 days.

The Figure 24 show the spatial distribution of the MPs whose time series are subject to trend variations regarding the mentioned parameters. The left part of the Figure 24 presents the MPs considering the unfiltered SNT SqueeSAR®. The right part of the Figure 24 also presents the seasonally filtered SNT SqueeSAR® results. Under the assumption that the seasonality is part of the normal temporal behaviour of the bridge, it will allow to detect other behaviour like settlement under a specific bridge.

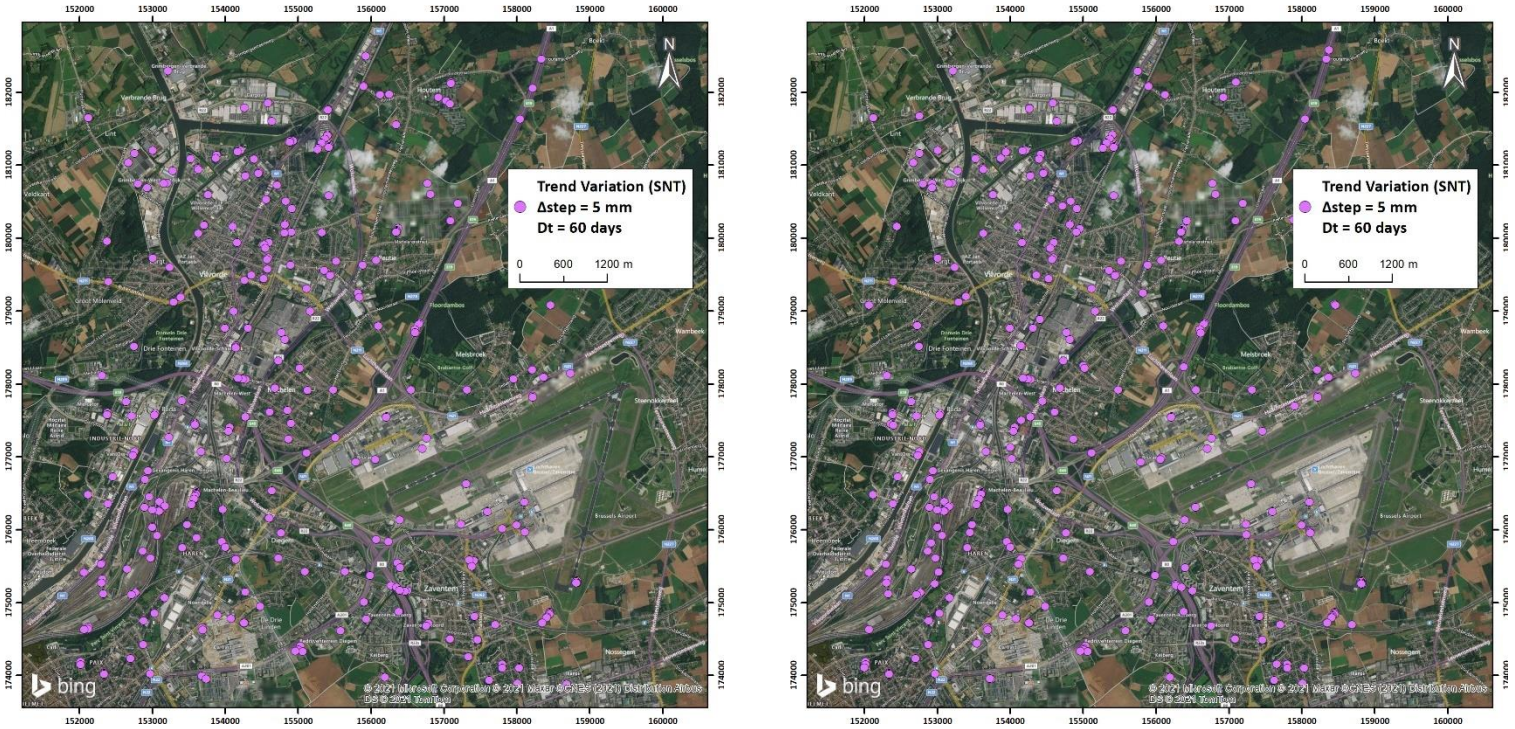

Figure 24: Left: TV analysis of the SNT SqueeSAR® analysis (Δstep = 5 mm, Dt = 60 days) with unfiltered results. Right: TV analysis of the SNT SqueeSAR® analysis (Δstep = 5 mm, Dt = 60 days) with results with filtered seasonal.

The Figure 25 shows examples of time series with unfiltered (left) and seasonally filtered (right) results. The time series on the left part shows that the algorithm can be triggered by seasonal signals (false positive). The time series on the right part shows an offset or abnormal behaviour detected by the algorithm on the seasonally filtered results.

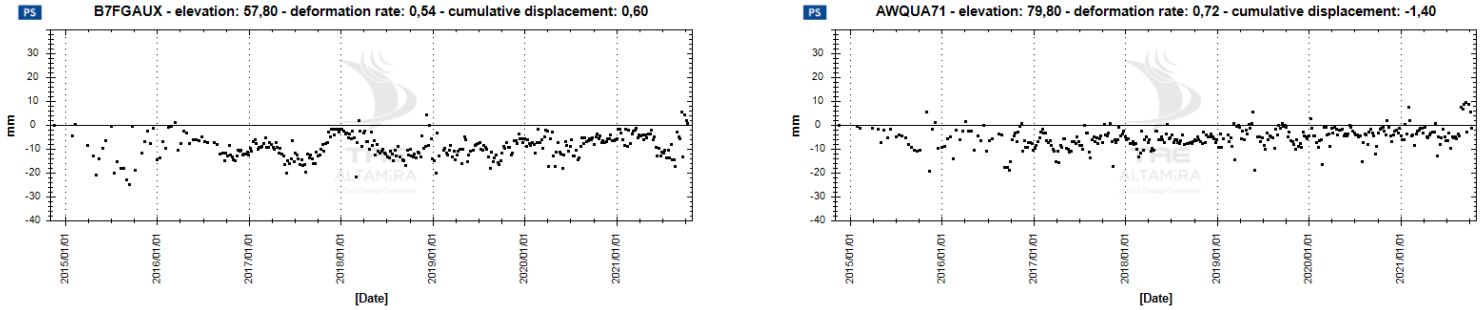

Figure 25: Left: SNT time series subject to trend variation (unfiltered). Right: SNT time series subject to trend variation (seasonally filtered).

Under the two approaches, no MP with a trend variation has been detected over any of the 21 bridges with the SNT SqueeSAR® analysis.

The Figure 26 shows the results for the TSX SqueeSAR® analysis with the same approach than the SNT images.

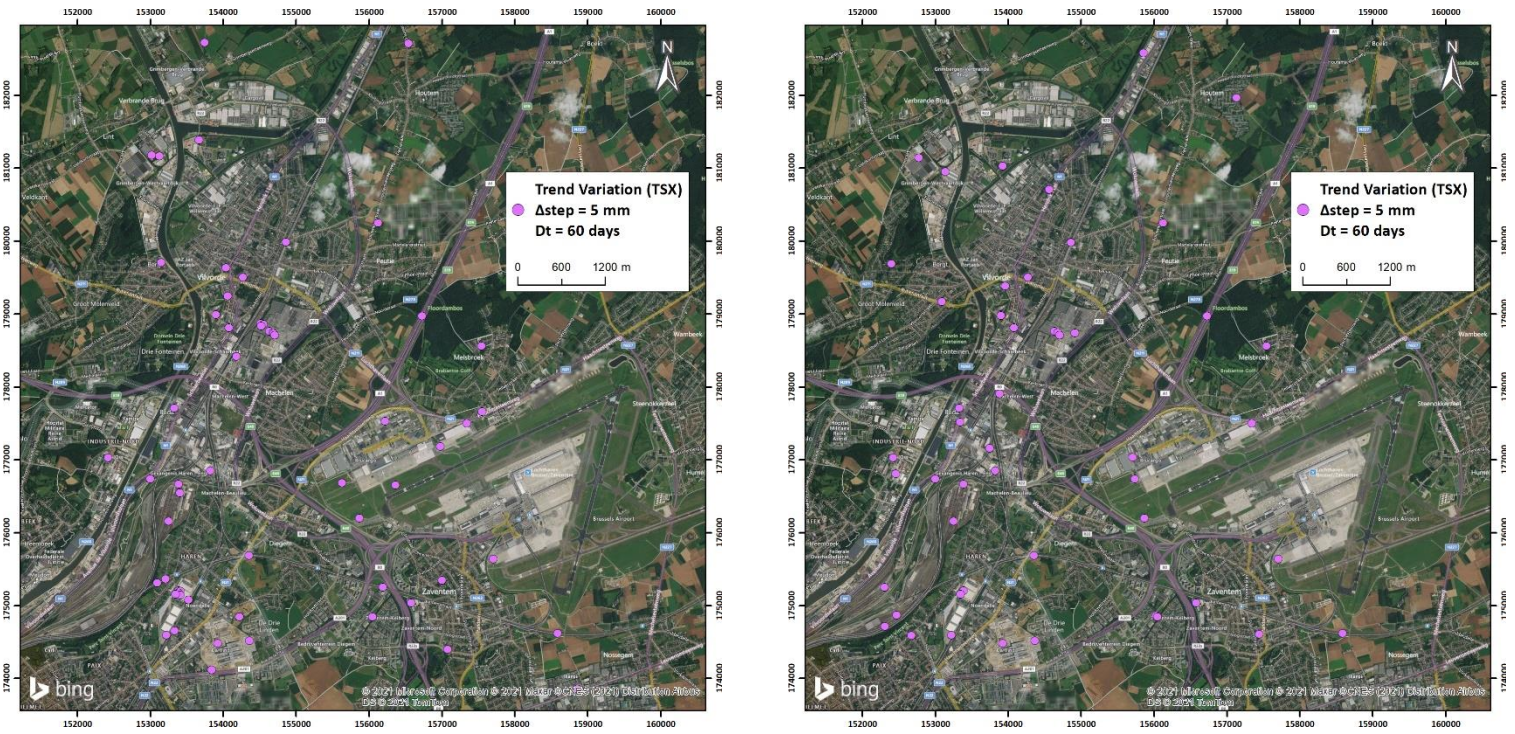

Figure 26: Left: TV analysis of the TSX SqueeSAR® analysis (Δstep = 5 mm, Dt = 60 days) with unfiltered results. Right: TV analysis of the TSX SqueeSAR® analysis (Δstep = 5 mm, Dt = 60 days) with results with filtered seasonal.

The analysis of the time series shows the results from the TSX SqueeSAR® analysis are less subject to false positive and more sensitive to small displacements (Figure 27). An offset (away from the satellite) with a value of ~7 mm is detected.

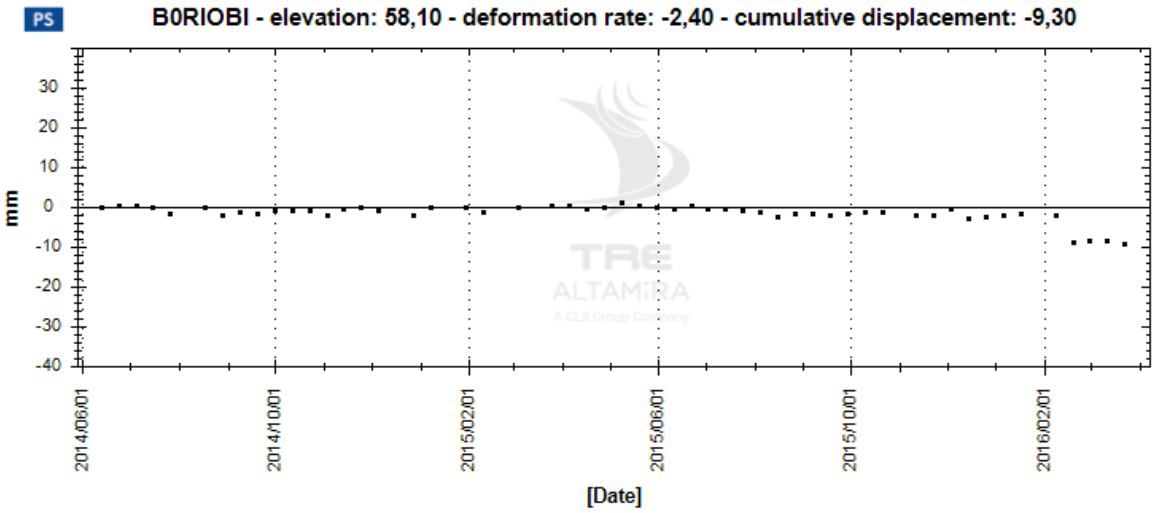

Figure 27: TSX time series subject to trend variation (unfiltered).

No MP with a trend variation has been detected over one of the 21 bridges with the TSX SqueeSAR® analysis using the aforementioned approach.

All these parameters are adjustable according to the client's needs.

5.3. Seasonal Change

As already described, SqueeSAR® results include the amplitude and phase of the displacement temporal series seasonal model, considering that these values come from the fitting of the model to the whole observation period. Using this concept, as a possible bridge control indicator, the seasonality evolution over different temporal spans can be investigated.

To that matter, employing the non-seasonality filtered SqueeSAR® results, a seasonal model can be fitted to the displacement series over consecutive yearly-based periods to study relative variations. This analysis has been carried out on the SNT SqueeSAR® due to its 7 years temporal coverage.

First, for every bridge database polygon provided by the client, the corresponding MPs having a larger seasonal amplitude value (coming from the SqueeSAR® results) than a certain threshold are selected. Afterwards, for each of those points, a seasonal model is fitted to the displacements over consecutive yearly-based periods, retrieving the amplitude and the phase of the seasonal model and their associated standard deviation. Depending on the number of samples and the noise present in the different yearly periods, the model parameters will have certain, and different, degree of uncertainty. Therefore, the standard deviation is needed in order to perform comparisons among the different intervals.

The described analysis is illustrated in Figure 28 and Figure 29 for points belonging to polygons 005843-001 and 005843-002, respectively. The upper figure contains, all MP above the mentioned threshold within the polygon, the displacement time series and their global seasonal model. The lower figure contains, for one point of the upper figure, the seasonal displacement pattern over the consecutive yearly basis periods with its corresponding amplitude and amplitude standard deviation (in mm). As seen in both lower figures, there are noticeable amplitude variations over different periods. No correlation with the local temperature (or any other factor) was carried out so we are not in the position of justifying such variations.

Different strategies (mainly driven by the client's guidelines) can be proposed in order to exploit such analysis and detect possible bridge anomalies. One could be extending it by synthetizing the relative amplitude variations (and their associated standard deviations) into a single "variation" parameter (after temperature correlation) and combining point's results at polygon level (assuming similar thermal response) getting

benefits for having larger spatial data samples. If proving to be a reliable methodology, it could be also considered as one of the parameters involved in the alert system.

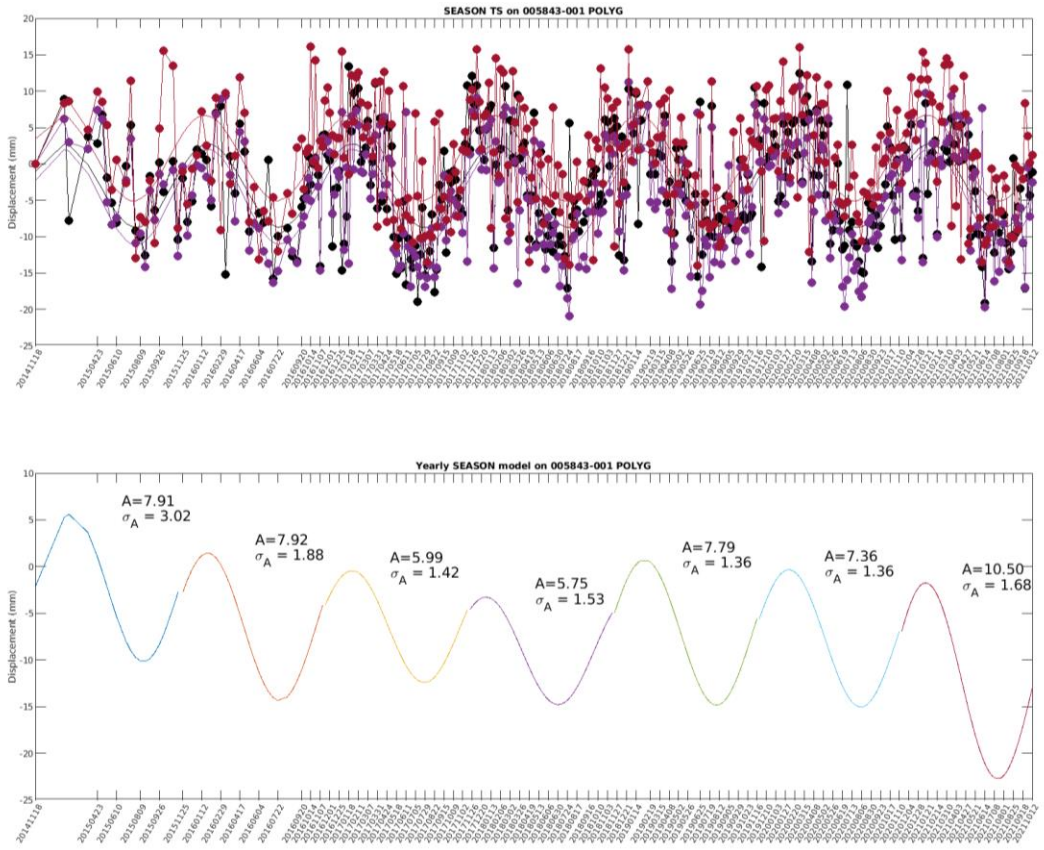

Figure 28: TSX Amplitude time series for all points belonging to polygon 003187-011. A one image duration significant amplitude change has been identified in all pixels.

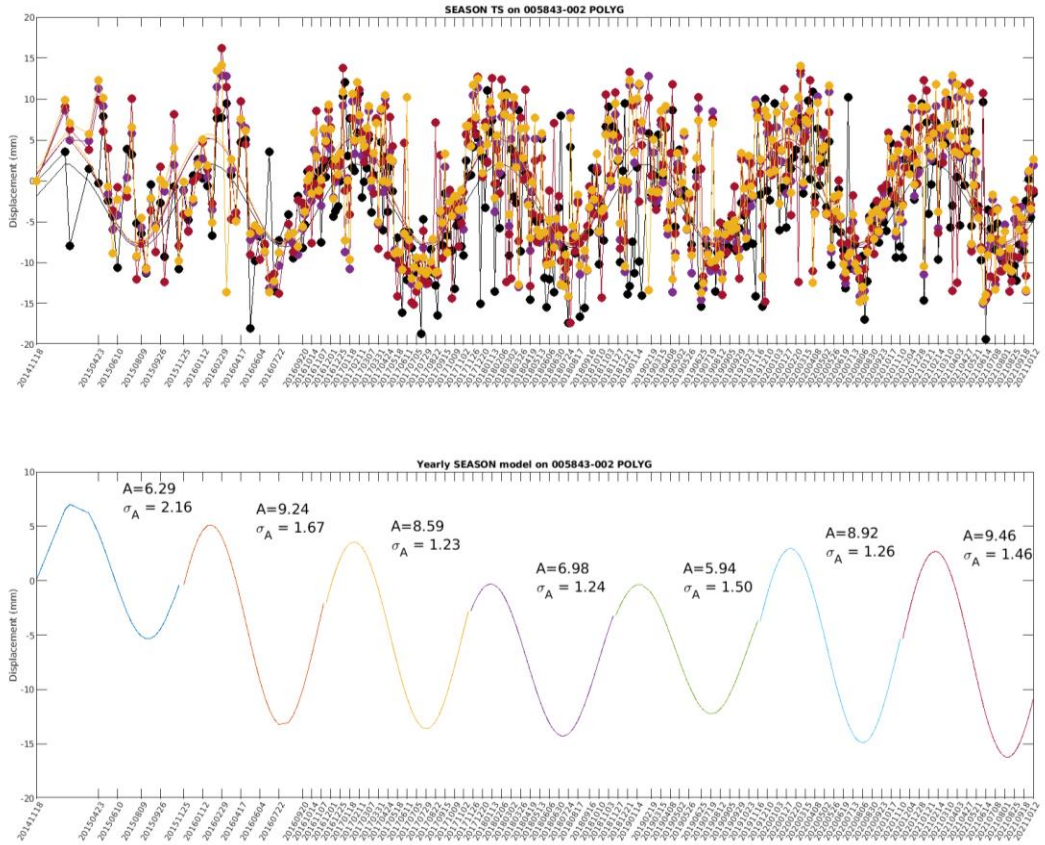

Figure 29: TSX Amplitude time series for all points belonging to polygon 003187-011. A one image duration significant amplitude change has been identified in all pixels.

5.4. Change detection over amplitude images

The amplitude of a SAR image is a measurement of the incident and backscattered energy rate over the illuminated target. Large amplitude values, appearing as brighter pixels, are those who backscatter to the SAR antenna almost all incident SAR signal. Low amplitude values, appearing as darker pixels are those whose incident SAR signal is spread over other directions in addition to the incident one, so just a small part of the incident signal is backscattered to the SAR antenna.

The amplitude value is driven by the geometry and type of material of the illuminated object. Therefore, if the object's geometry is significantly modified, a change on the amplitude values arises. Based on this principle, the amplitude temporal series is analyzed for every pixel. After a statistical analysis, the probability of having a significant relative amplitude change is calculated for all the images so those overpassing a threshold value are detected identifying the date of the change.

The type of change can be roughly summarised in temporal or permanent. In the temporal one, once the change is detected, the initial amplitude behaviour is recovered after one or few dates. If permanent, after the significant amplitude change, the new amplitude behaviour remains until the end of the observation period. Typically, the temporal one would concern construction works which temporary modify the geometry or materials of the area, setting back the initial spot physiognomy after the intervention. On the contrary, the permanent one is typically related with a major geometry or material work which permanently changes the physiognomy of the spot.

The result of this study is valuable for mainly two purposes. The first one is to identify major "physiognomy" actions on the bridge, even though it is assumed that the client has knowledge of them. In any case, this study would be of interest in order to better characterise which type of works are significant in SAR terms to affect the SAR amplitude to be sensitive enough to detect the associated change. The second one deals with the impact of these changes on the phase quality and thus the displacement results. Suppose that the surface has been significantly modified (from temporally coherent to temporally non-coherent) for a shorter period than the whole timespan. In that case, the corresponding pixels may still be detected in the SqueeSAR® dataset but the displacement samples of the affected dates are susceptible of being noisier. The amplitude study would then help to identify these areas and affected images.

In order to illustrate the methodology and the associated results, the described analysis has been carried out on SqueeSAR® TSX and SNT MPs belonging to the bridge's polygons where construction works took place, as provided by the client. This temporal amplitude analysis, if considered of interest, can be extended to all the points belonging to the corresponding polygons, not only to those contained in the SqueeSAR® database.

No significant changes were identified in the SNT dataset while in the TSX dataset few cases of significant changes on the amplitude time series were identified. In particular, one temporary and one permanent on 003187-011 and 003187-005 polygons, respectively, both illustrated in Figure 30 and Figure 31. The first case shows a one image duration temporary change located on the 2015.06.11, behaviour followed by all pixels but one belonging to that polygon. The second one illustrates a permanent significant change after 2015.03.04 on the single pixel belonging to that polygon. There, the amplitude changes from low to large backscatter. According to the available information, the 003187 polygon renewed its bridge deck in 2016 (the exact dates were not specified), so both changes could not be justified by that action.

Two more cases were identified in the 009105-004 and 0091-005 polygons, both illustrated in Figure 32 and Figure 33. In the first one, two out of the three pixels located within the 009105-004 polygon show a low to large amplitude change after 2014.11.14. In the second one, some significant changes are placed within the 2014.08.18-2015.01.30. According to the available information, restoration works took place from 2014.08.01-2015.02.15 took place in polygon 009105, so especially in the second case, some correlation

between the amplitude changes and the works could happen. In any case, further investigations are required to have more solid conclusions.

This information, either as pixel based similar to the SqueeSAR® database (even being one of its fields) or performing some polygon based statistical analysis, could be provided if being of interest to the client.

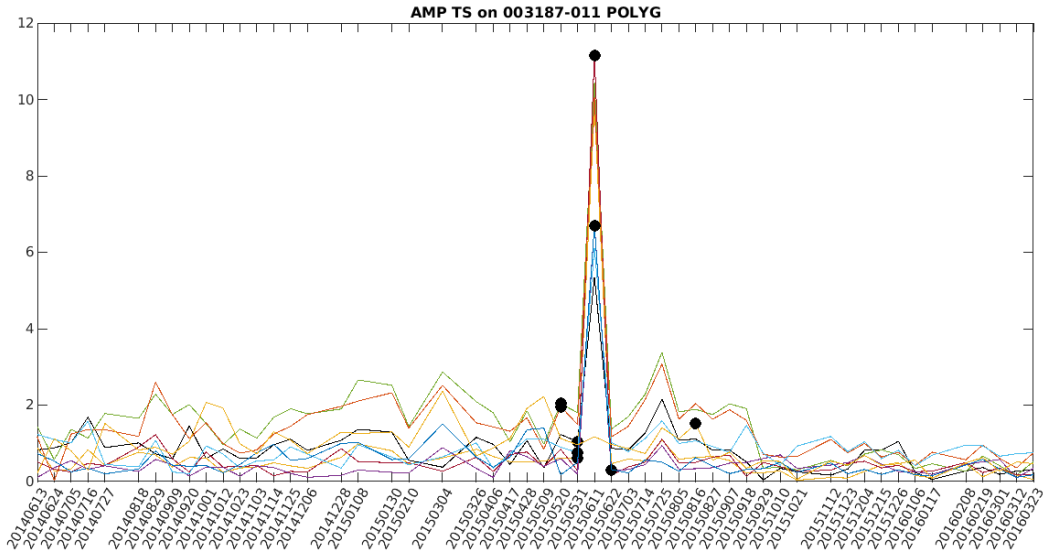

Figure 30: TSX Amplitude time series for all points belonging to polygon 003187-011. A one image duration significant amplitude change has been identified in all pixels.

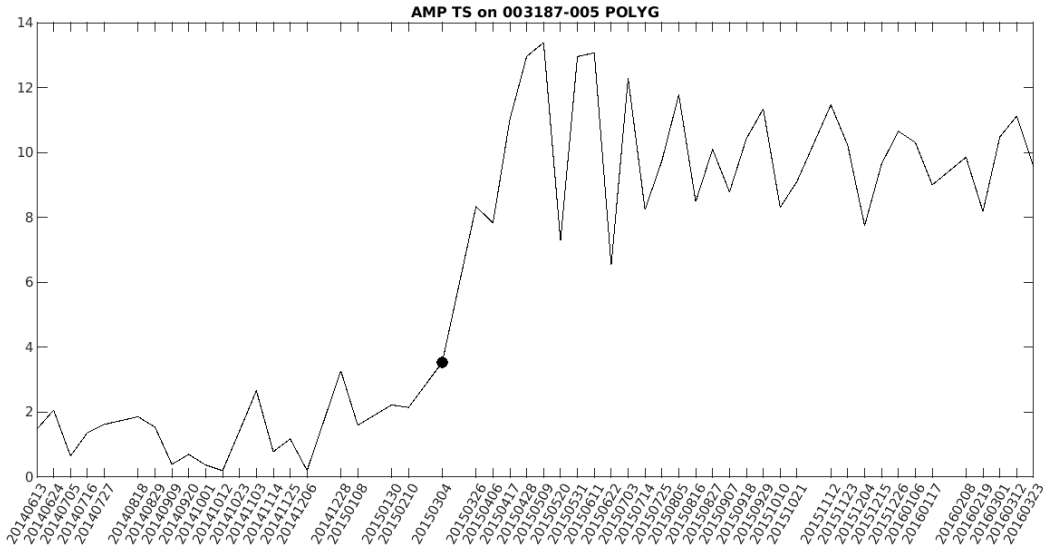

Figure 31: TSX Amplitude time series the single point belonging to polygon 003187-005. A permanent significant amplitude change has been identified from 20150304 on.

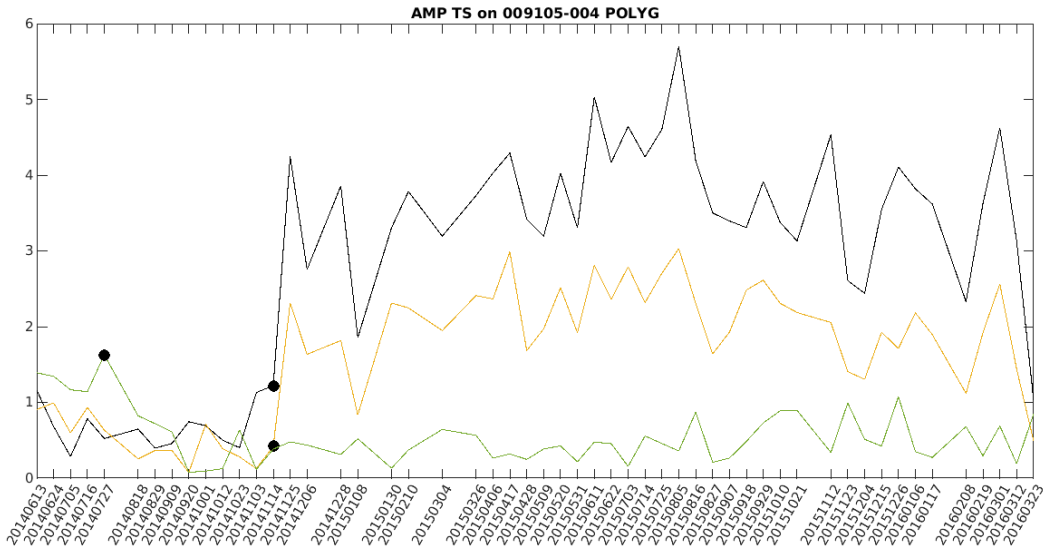

Figure 32: TSX Amplitude time series for all points belonging to polygon 009105-04. On two of the three polygon's pixels present a permanent amplitude change from 20141114.

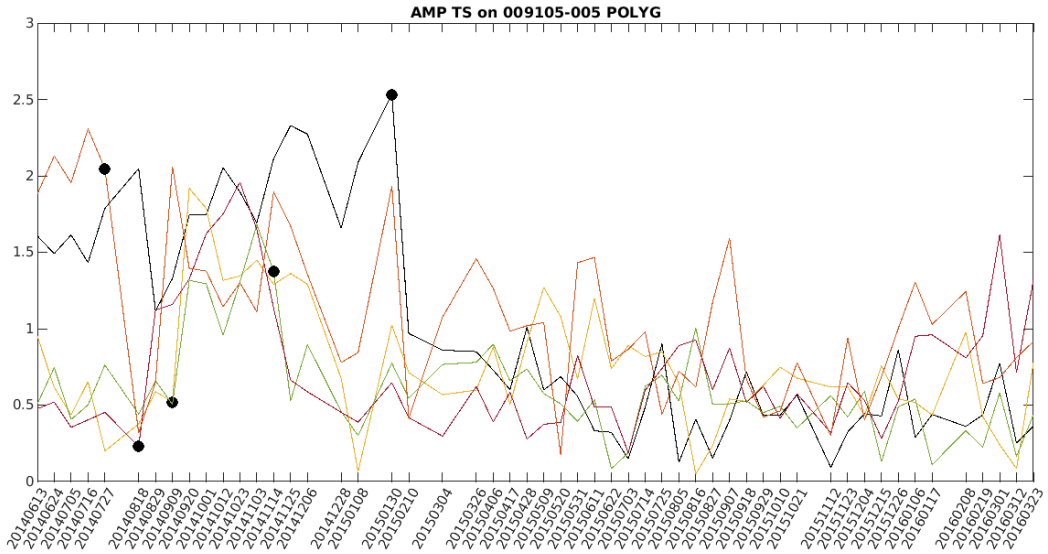

Figure 33: TSX Amplitude time series for all points belonging to polygon 009105-05. On two of the three polygon's pixels present a permanent amplitude change from 20141114.

5.5. Alerting system

In order to characterize the motion behavior at a bridge component level, a polygon analysis is performed over the point-like SqueeSAR® results. The SqueeSAR® points belonging to the bridge's polygons provided by the client are identified and different statistics are calculated over the values contained in the SqueeSAR® results shapefile fields. The mean, the standard deviation, the maximum value, the minimum value, certain percentile, etc., can be calculated considering the displacement and/or the velocity. We believe that this grouping, complementary to the point-wise analysis, helps to better identify significant episodes among parts of the bridge sharing structural properties.

A prototype of alerting system has been designed during this Proof Of Concept phase, by taking advantage of the polygon analysis (with shapefiles of the bridges provided by the client). The objective is to design an adaptative alerting system depending on the SqueeSAR® analysis. As for the Trend Variation analysis in section 0, we assume that the seasonality is part of the normal temporal behaviour of the bridge. The results then filtered have been used for the alerting system. It is based on the averaged deformation (corresponding to the period of analysis for each satellite) associated with each polygon.

The statistical distribution of each deformation value associated with each polygon is analysed regarding the SqueeSAR® analysis (138 elements for SNT and 245 elements for TSX). We assume that the deformation values follow a normal distribution, we consider the statistical distribution example shown on the Figure 34.

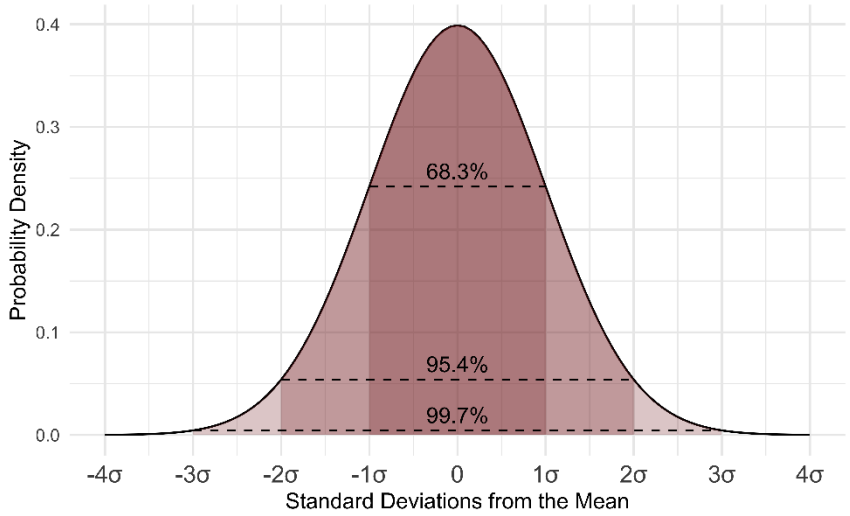

Figure 34: Example of a normal distribution.

For each SqueeSAR® analysis and the averaged deformations d, we consider their mean value m, and their standard deviation σ. The following test t is performed:

$$t = |d - m|$$

If $t < \sigma$, the section of the bridge symbolised by the polygon is out of concern.

If $\sigma \leq t < 3\sigma$, the section of the bridge symbolised by the polygon is matter of concern.

If $t \geq 3\sigma$, the section of the bridge symbolised by the polygon is considered in alert.

The following Figure 35, Figure 36, and Figure 37 present the results over different cases: a steel bridge with a long deck (Viaduct van Vilvoorde), a steel bridge with a small deck, and a concrete bridge in two parts, respectively. The values for the SqueeSAR® SNT analysis are:

- $m = -1\ mm$
- $\sigma = 6$ mm

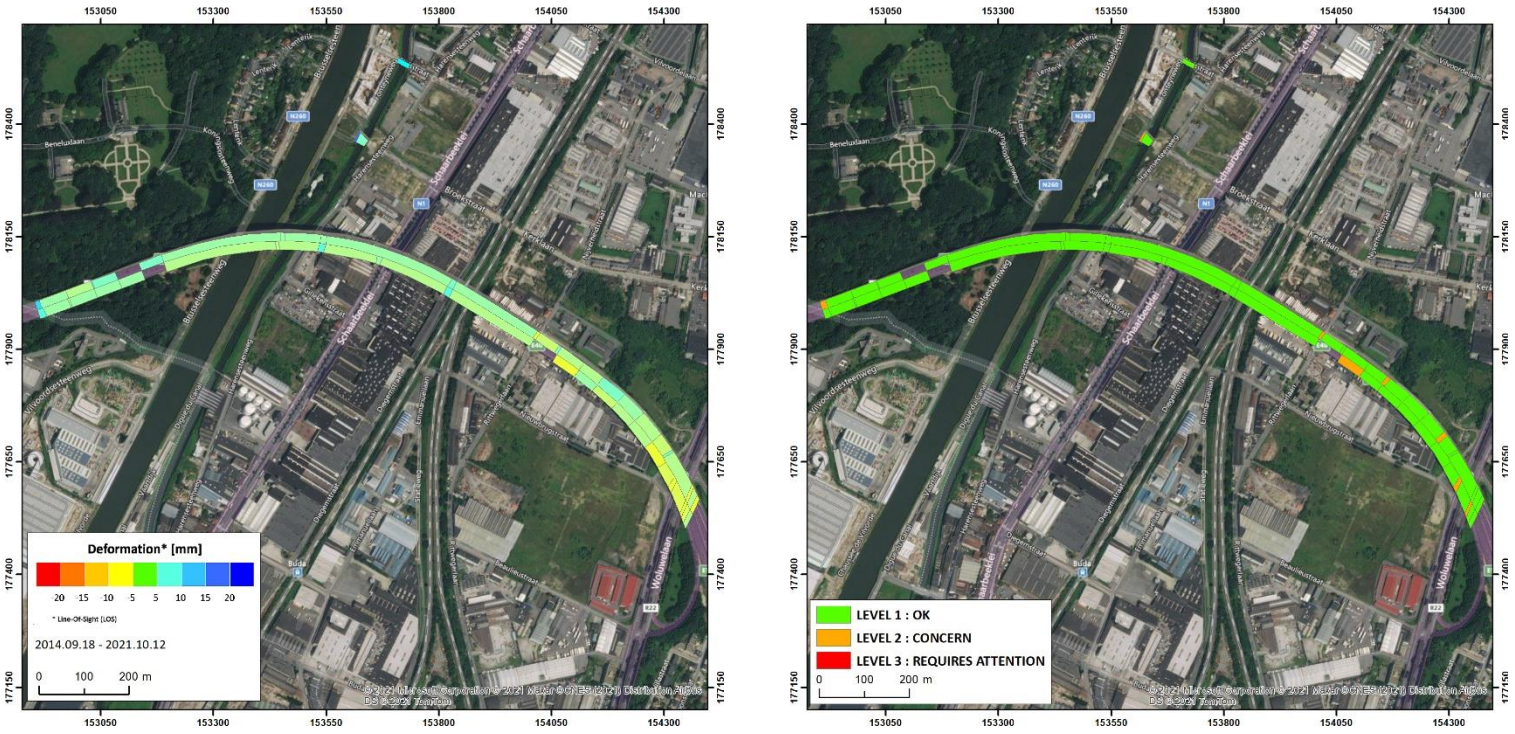

Figure 35: Left: SNT SqueeSAR® deformation (mm) in function of the polygons over the Viaduct van Vilvoorde. Right: Corresponding alerting system.

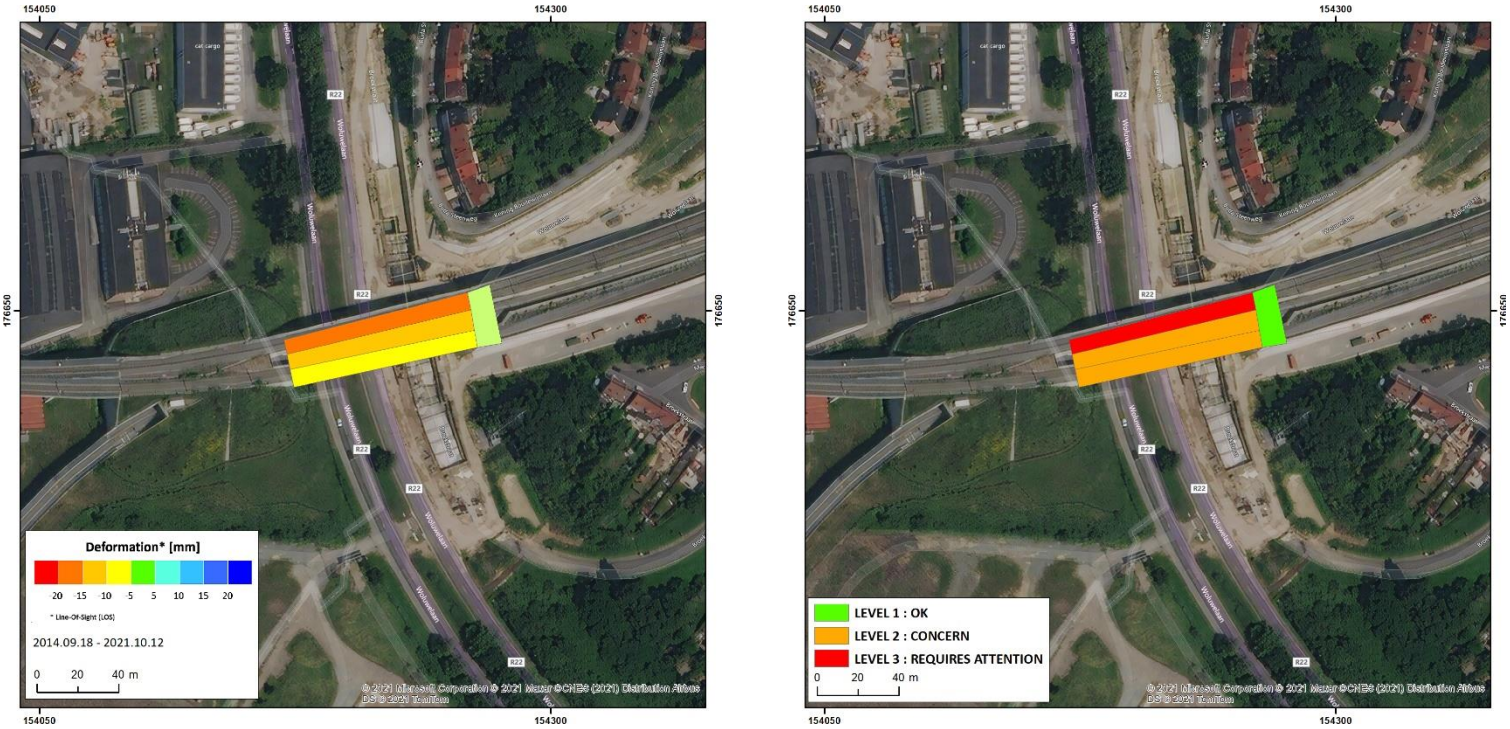

Figure 36: Left: SNT SqueeSAR® deformation (mm) in function of the polygons over a steel bridge. Right: Corresponding alerting system.

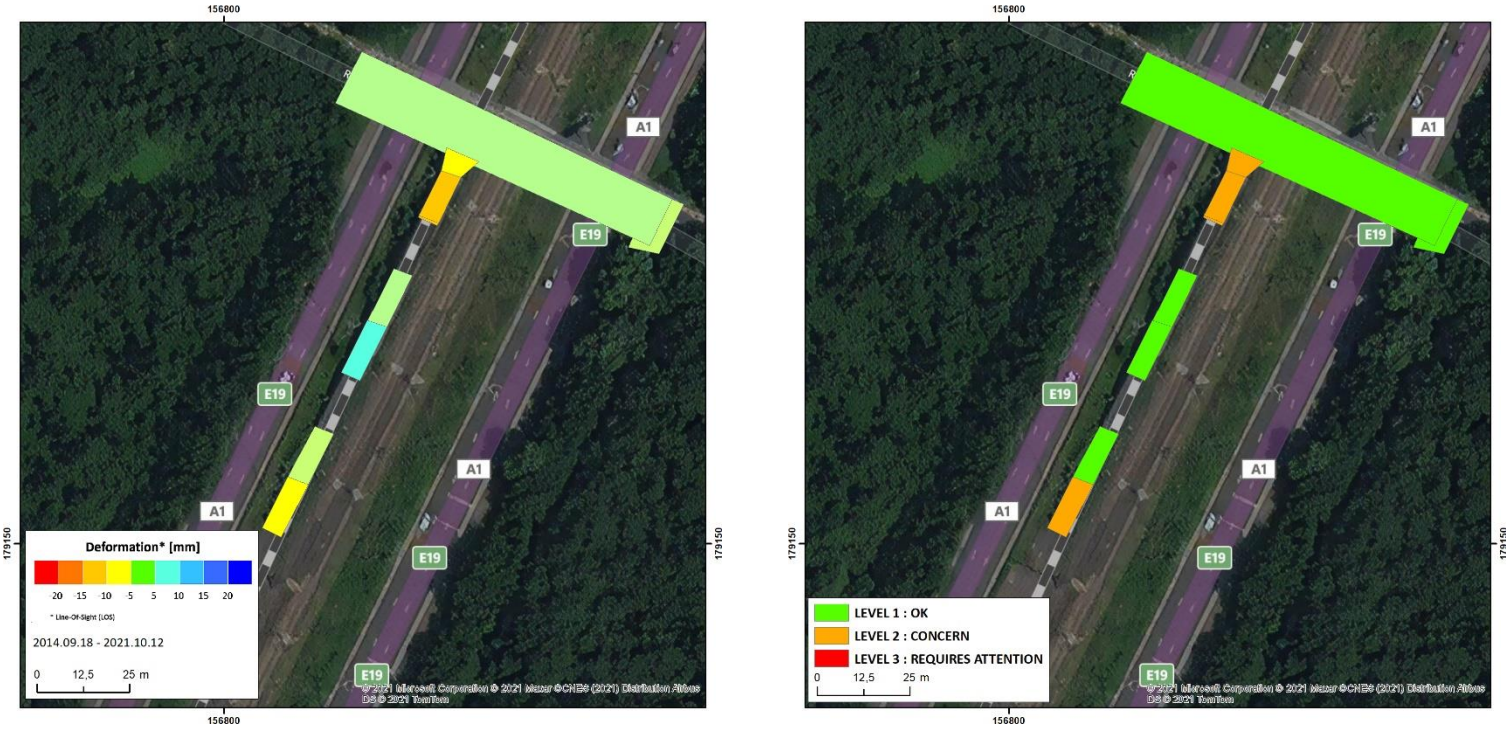

Figure 37: Left: SNT SqueeSAR® deformation (mm) in function of the polygons over a concrete bridge. Right: Corresponding alerting system.

The following Figure 38, Figure 39, and Figure 40 present the results over the same bridges than the SNT results with SqueeSAR® TSX analysis. The values for the SqueeSAR® TSX analysis are:

- $m = 0\ mm$
- $\sigma = 2$ mm

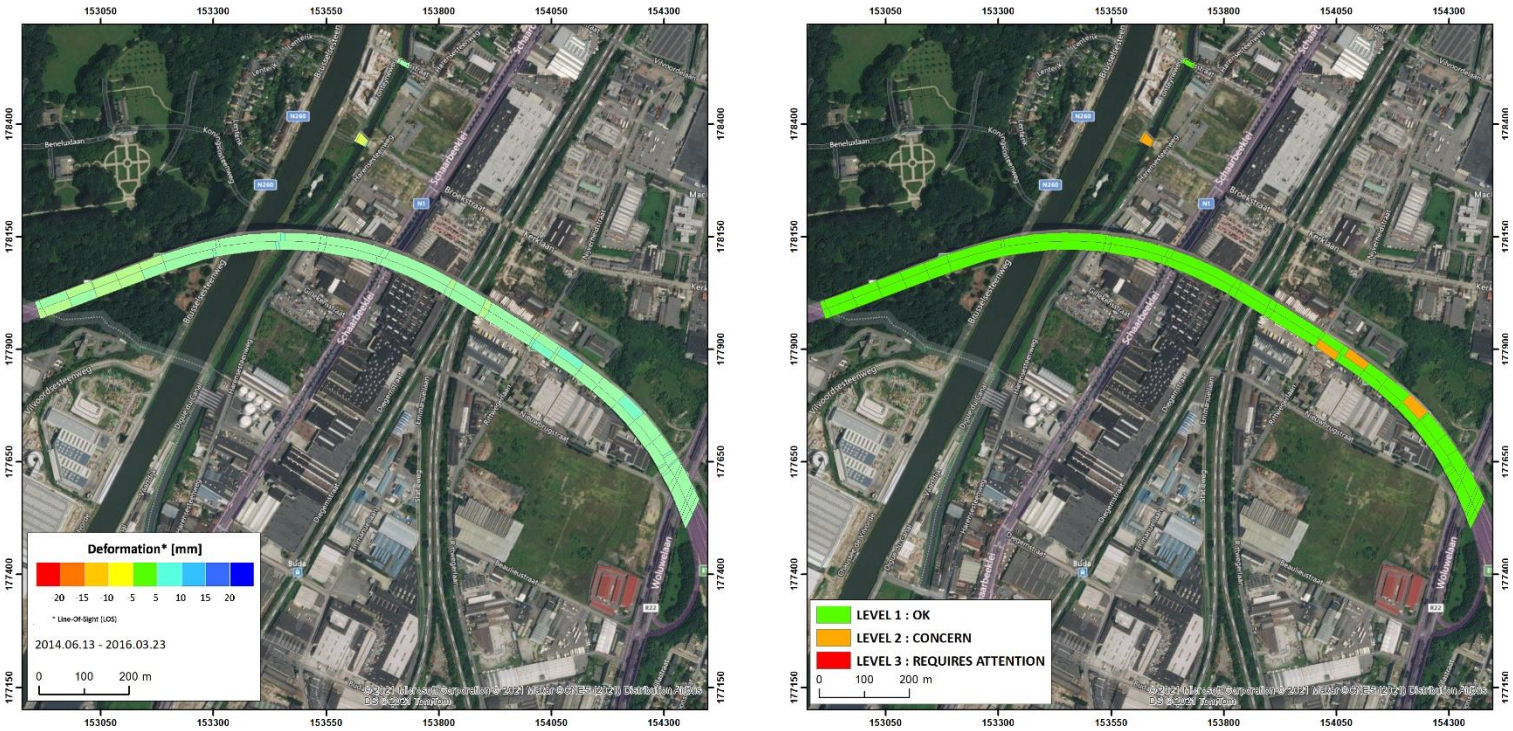

Figure 38: Left: TSX SqueeSAR® deformation (mm) in function of the polygons over the Viaduct van Vilvoorde. Right: Corresponding alerting system.

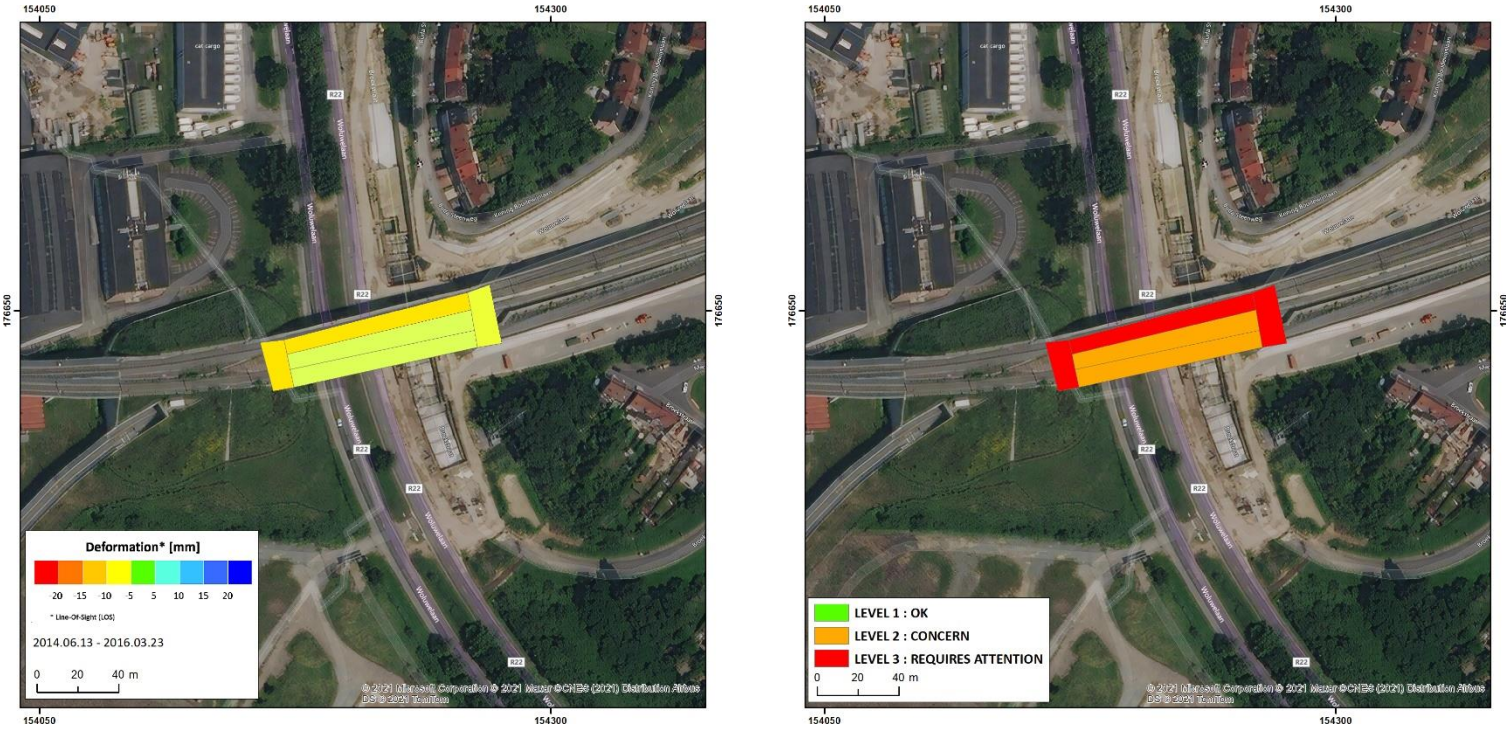

Figure 39: Left: TSX SqueeSAR® deformation (mm) in function of the polygons over a steel bridge. Right: Corresponding alerting system.

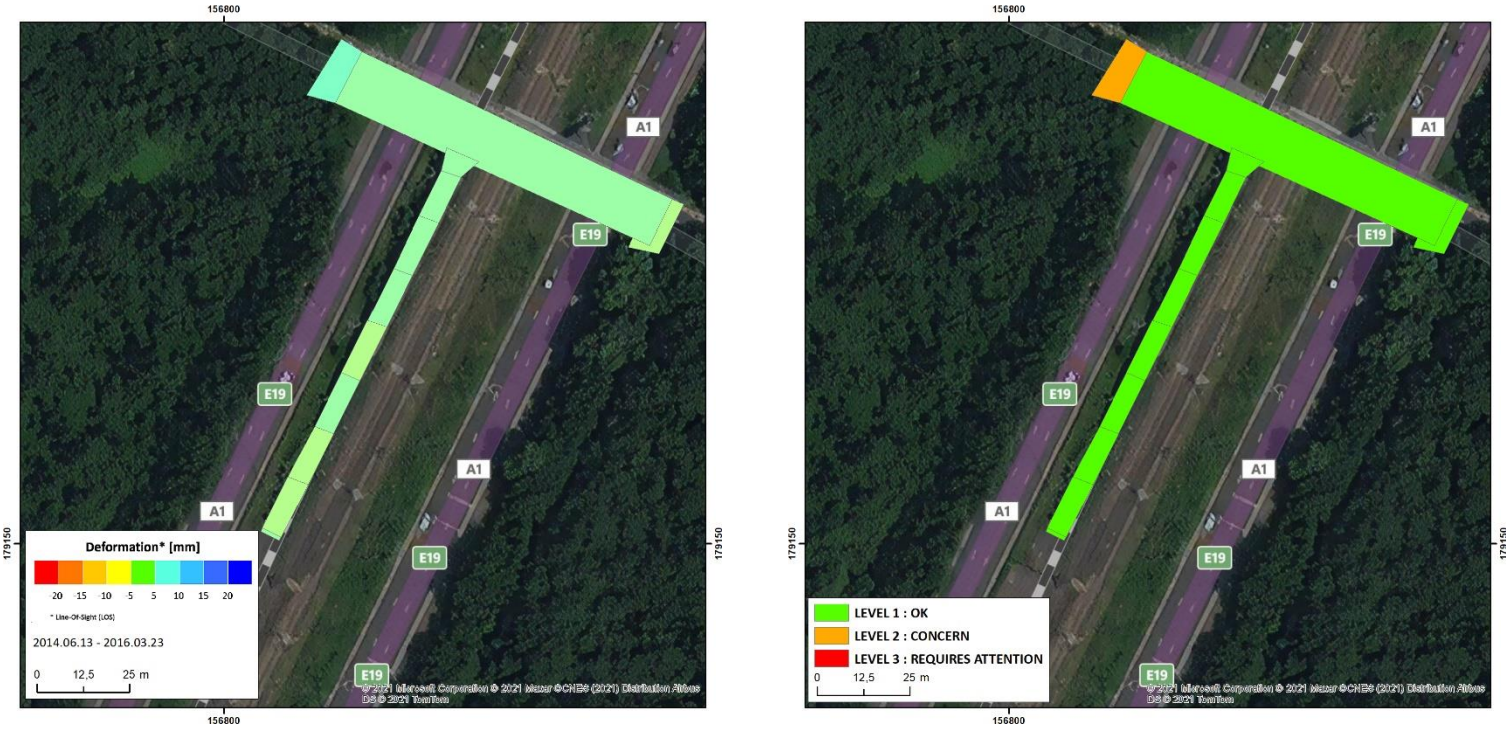

Figure 40: Left: TSX SqueeSAR® deformation (mm) in function of the polygons over a concrete bridge. Right: Corresponding alerting system.

Further analysis can be performed according to the client's needs. The previous statistics can be estimated in function of the material of the bridge (steel or concrete for example) or the structure (abutment or deck for example).

5.6. In-depth analysis where no measurement points are available

Geometrical distortions and vegetation coverage, together with the previously mentioned reflectivity changes and complex motion patterns, are among the reasons why an area may not behave as a reliable InSAR point (PS or DS), thus showing a lack of information.

Vegetation typically affect InSAR results negatively by decreasing the measurement point density and creating noisy results, however some vegetated areas can still provide reliable results and valuable information.

Different areas where no or few measurement points can be observed in this Proof Of Concept. Most of the areas affected by the lack of measurement points are vegetated areas (forests, gardens or cultivated fields). The phenomenon is also observed in artificial areas. The presence of construction works that can change the nature or reflectivity of the ground during the period of analysis can generate a loss of interferometric

coherence and therefore a lack of measurement points in the area. An example is given in the Figure 41 below: one of the parking lots located in the airport area underwent heavy construction work during the year 2015 (included in the 2014-2016 TSX period), generating a loss of measurement points in the area.

Figure 41 : Up: Area where construction works occurred during the studied period. Down: Same area where SqueeSAR® analysis does not provide a large amount of measurement points

6. Comparison of the use of Sentinel-1 and TerraSAR-X images

The objective of this section is to review the impact of using SNT or TSX images in this study for bridge deformation monitoring. The following points are listed below. An important reminder is that the period of analysis of the SNT and TSX SqueeSAR® analysis are different, about 7 years against 2 years. It would have a beneficial impact for the SNT SqueeSAR® in terms of MP reliability and a beneficial impact for the TSX SqueeSAR® analysis in terms of spatial coverage.

- **Accuracy**: The acquisition wavelength of SAR images allows theoretically to reach a millimetre accuracy. The variance of phase observation is proportional to the wavelength of the satellite (Pepe and Calò, 2017). When working with different acquisition wavelengths (5.66 cm for C-band data and 3.10 cm for X-band data), it is expected to detect smaller displacements with the smaller acquisition wavelength.
- **Spatial resolution**: The X-band images (TSX) have a higher spatial resolution than C-band images (SNT). The pixel size is about 3x3 m against 20 x 5 m. This results in a higher MP density, 2417 MP/km² against 20 240 MP/km² which is more suitable for infrastructure monitoring.
- **LOS angle θ**: The LOS angle as an impact on the comprehension of the results in the case of a 1D study. This angle is lower for the TSX SqueeSAR® (θ = 20.86°) than the SNT SqueeSAR® results (θ = 38.84°). It allows an easier direct comparison with the levelling data for the TSX results when the SNT results will need further processing (2D decomposition) in order to be properly compared with ancillary data.
- **Atmospheric correction**: As mentioned in the section 2.1 and the section 2.3, a high spatial distribution of the MPs allows a better estimation of the atmospheric contribution, and thus reduce the noise level on the estimate of displacements. Furthermore, a lower LOS angle implies a shorter passage of the signal in the atmospheric layers and thus a lower atmospheric contribution.
- **Data availability**: From an operational perspective, the TSX images are more suitable for deformation monitoring because they are tasked over a dedicated area, a specified period, and an acquisition frequency. The SNT images acquisition is managed by ESA.

The TSX images are more suitable for infrastructure monitoring because of their sensitivity to small displacements, spatial resolution, and MP density. Moreover, a lower LOS angle allows a faster comparison with ancillary data and a lower atmospheric contribution. From an operational perspective, the images acquisition is ensured once they are tasked for the monitoring over a dedicated area.

However, SNT images allows to assess a better state of art of displacement because of availability and free of charge. An analysis with descending and ascending geometry also allows to conduct a decomposition of the true Vertical and East-West displacements.

7. Conclusions

In the scope of this Proof Of Concept, performed for the Flemish public administration (Department of Mobility and Public Works / Geotechnics Division), 21 bridges of different material, structure and year of construction have been studied. They are located within an AOI of 55 km² located in the north of Brussels.

A state of art of the deformation has been set using the patented SqueeSAR® algorithm in order to perform an InSAR analysis over the entire area. Two datasets have been used, 349 Sentinel-1 images from November 18th, 2014, to October 12th, 2021; and 53 TerraSAR-X images from June 13th, 2014, to March 23rd, 2016.

The amount of information that can be extracted from the SqueeSAR® results has been demonstrated in this technical report. Information can be used directly such as the deformation, deformation rate, and seasonal amplitude. Time series and deformation profiles can be generated from the measurement points on-the-flight via the TREmaps® visualisation platform.

TRE ALTAMIRA associates to this technical report 42 monographs that can be downloaded on the TRE ALTAMIRA's platform, TREmaps®. These 42 monographs correspond to the individual analysis of each bridge for each satellite solution used within this project.

Further products have been generated for the needs of this project such as the analysis of the surroundings of the structures in order to extract only the measurement points on the bridges. Moreover, Trend Variation maps have been generated in order to identify measurement points affected by sudden changes. Change Detection analysis over the amplitude images have also been performed in order to detect measurement points affected by loss or change of backscattered signal (due to construction works for example). Finally, a 3-level alerting system has been designed based on the polygons of the bridges provided by the client. They are colour-coded (green: out of concern, orange: preoccupation, red: alert) in function of the averaged deformation of the measurement points within them.

8. References

Pepe, A., and Calò, F., 2017. A Review of Interferometric Synthetic Aperture RADAR (InSAR) Multi-Track Approaches for the Retrieval of Earth's Surface Displacements, *Applied Sciences*, **7(12)**, 1264.

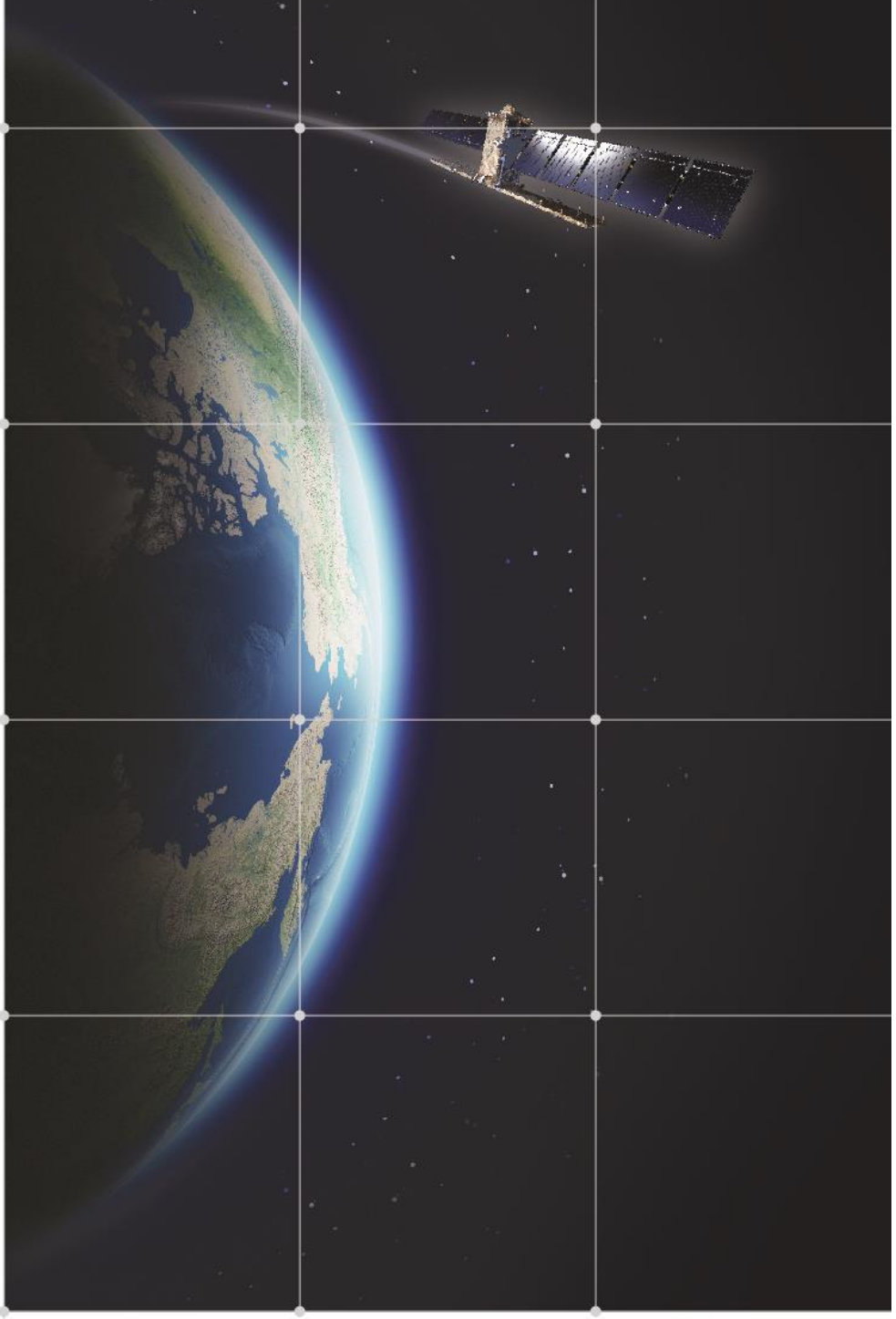

TRE ALTAMIRA
A CLS Group Company

MILAN

Ripa di Porta Ticinese, 79
20143 Milano - Italy
Tel. +39.02.4343.121
Fax +39.02.4343.1230

BARCELONA

C/ Corsega, 381-387
E-08037 Barcelona Spain
Tel.: +34 93 183 57 50
Fax: +34 93 183 57 59

VANCOUVER

410 - 475 West Georgia Street
Vancouver, BC V6B 4M9 - Canada
Tel. +1.604.331.2512
Fax +1.604.331.2513

tre-altamira.com